Ore Geology Reviews 89 (2017) 270–289

Contents lists available at ScienceDirect

Ore Geology Reviews

journal homepage: www.elsevier.com/locate/oregeo

Genesis of manganese deposits in southwestern Amazonia: Mineralogy, geochemistry and paleoenvironment

Márcio Fernando dos Santos Albuquerque [a,*], Adriana Maria Coimbra Horbe [b], Nilson Francisquini Botelho [b]

[a] Graduate Program in Geology, Brasilia University, Geoscience Institute, Darcy Riberio University Campus, 70910-900 Brasília, Federal District, Brazil
[b] Brasilia University, Geoscience Institute, Darcy Riberio University Campus, 70910-900 Brasília, Federal District, Brazil

ARTICLE INFO

Article history:
Received 29 September 2016
Received in revised form 5 June 2017
Accepted 9 June 2017
Available online 16 June 2017

Keywords:
Coronadite
Pb-hollandite
Romanechite
Hydrothermal
Lateritic duricrust

ABSTRACT

Chemical analysis, XRD, SEM and EMPA were carried out on five manganese deposits in southwestern Amazonia, Brazil to determine their sources of Mn, their lithostratigraphic units, the environment in which Mn accumulated during the Proterozoic and the effects of weathering (since the Late Cretaceous) on the mineralization process. The sedimentary, hydrothermal and lateritic environments in this area produced a wide and complex variety of structures, textures, minerals and geochemical features, where coronadite, hollandite and romanechite, as the main Mn-minerals, changed their chemical compositions during the lateritization process. In this context, during lateritization, more mobile elements (MgO, CaO, Na_2O and K_2O) were removed, while concentrations of SiO_2, Al_2O_3, Fe_2O_3, MnO, Pb and Co increased. The high concentrations of Cu, Pb, and Tl and the presence of positive Gd anomalies, galena, and nuggets of Ag and (Zn/Ni)/MnO_2 in both the protoliths and duricrusts indicate that the Zé Julião, Apuí and Novo Natal deposits record the influences of sulfide and hydrothermal activity. The REE/(Zr/Hf) vs $TiO_2 \times 1000$/(Co/Ni) ratios indicate that felsic and mafic rocks were the sources of Mn in these samples.

1. Introduction

The mineralogical and geochemical parameters of manganese minerals are useful for paleoenvironmental reconstructions of the evolution of the atmosphere, the chemical compositions of ancient oceans and the pH and Eh variations of depositional environments. Additionally, they may have implications for their geochemical environment, due to the ability of manganese to adsorb elements such as Ba, Pb, Co, Cu, Ni, Ag and Zn (Frakes and Bolton, 1992; Nicholson, 1992; Roy, 1992, 2006; Conly et al., 2011; Del Rio-Salas et al., 2013).

Mn-enriched zones are derived from sedimentary, metasedimentary and hydrothermal rocks and their weathered equivalents; they range in thickness from a few meters to over 50 m and laterally extend from a few meters to over 50 km (Force et al., 1999).

Mn that is hosted in sandstones, greywackes, shales and conglomerates and is associated with BIFs tends to form large to giant deposits (with average values of 51 Mt and 31% MnO) (Roy, 2006; Maynard, 2010). When Mn sedimentary sequences are metamorphosed, their primary minerals are converted into Mn silicates or Mn carbonates (e.g., rhodonite, spessartite, Mn calcite, tephroite) and they can form small or large deposits (<1 Mt to 43 Mt) (Roy and Purkait, 1968; Rodrigues et al., 1986; Nicholson et al., 1997; Chisonga et al., 2012). On the other hand, Mn deposits that are associated with hydrothermal environments are rather small (< 4 Mt), because they are mostly restricted to epithermal zones and occur as veins, breccias and irregular orebodies (O'Really, 1992; Glasby et al., 2001; Liakopoulos et al., 2001; Leal et al., 2008; Conly et al., 2011). The latter type of Mn deposit, which occurs in the ocean floor and within ophiolite complexes, has a particular geochemical composition and can be used to understand the behavior of Mn in plate boundary zones. The circulation of warm water through fractures removes Mn, Fe, Pb, Zn, Cu, Co and Ni from volcanic rocks, thus forming deposits with large varieties of Mn minerals (Roy, 1992, 1997; Maynard, 2014).

All of these types of Mn environments, when subjected to weathering, generate supergene Mn ores with mineralogies and geochemical compositions that are associated with the type of Mn-bedrock that was weathered (Nicholson, 1992). Generally, Mn orebodies are mined from Mn-rocks or Mn-lateritic duricrusts (Rodrigues et al., 1986; Pracejus, 1989; Pracejus and Bolton, 1992; Chisonga et al., 2012). When supergene Mn develops from a sulfide mineralization sequence, it is classified as dubhite (Nicholson,

* Corresponding author.
E-mail address: mgeoroots@gmail.com (M.F.S. Albuquerque).

http://dx.doi.org/10.1016/j.oregeorev.2017.06.012
0169-1368/

1992) and can be used as a tool for sulfide surveys, due to the formation of Mn-minerals that are enriched in trace elements, such as coronadite, hetaerolite, chalcophanite, crednerite and Pb-hollandite.

In southwestern Amazonia, Brazil, there are 261,300 ha that require examination in Mn studies, where Mn is associated with the sedimentary rocks and lateritic duricrusts of the Sumaúma Supergroup (Liberatore et al., 1972; Gonçalves and Serfaty, 1976; Fig. 1). Among them, only 179 ha have been investigated by BBM Amazonas Ltd. (using trenches, wells and galleries) in seven potential Mn-rich areas that contain 3.52 Mt of Mn (Cotovelo, Beneficente, Rosinha, Fazenda Floresta, Novo Natal, Pretinho and Zé Julião; Fig. 1). This paper describes the features of these Mn deposits and their occurrences related to sedimentary, hydrothermal and supergenic environments, which may represent the 7.8% of Mn deposits (Maynard, 2010) that have unusual mineralogies (i.e., romanechite, hollandite and coronadite) and geochemical compositions compared to the largest Mn deposits (e.g., Rodrigues et al., 1986; Okita, 1992; Pracejus and Bolton, 1992; Cornell and Schutte, 1995; Gutzmer and Beukes, 1996; Costa et al., 2005). In this study, these data facilitated the recognition of the Mn source and its mineral and chemical transformations due to the influence of lateritization. This study also discussed the genesis of Mn ore, which helped improve the geological

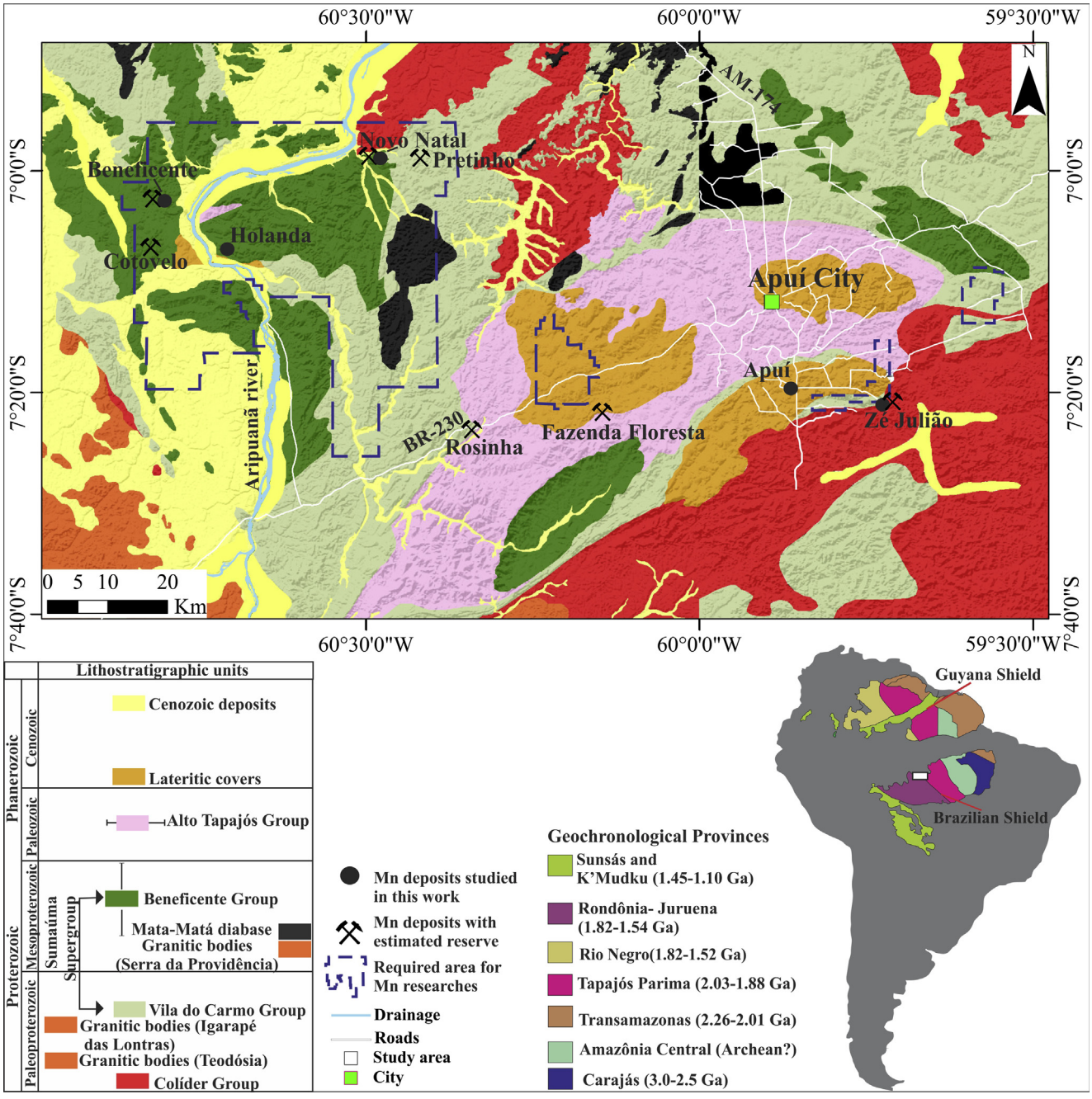

Fig. 1. Localization of study area and geological setting. Geological map carried out for CPRM (2013) (Geological Service of Brazil), still under revision (red square).

knowledge of Proterozoic rocks in Amazonia and highlight the potential of VMS mineralization in this region. Moreover, this paper proposed a new method of genetic classification and a new method to estimate the amount of Mn-minerals present using geochemical and XRD data.

2. Environmental and geological setting

The study area is located in the southwestern region of Amazonia, Brazil, between 6–13°S and 59–62°W (Fig. 1). The climate is hot and humid and is slightly drier from May to September. The mean annual temperature ranges from 25 to 27 °C, the relative humidity is approximately 85%, and the yearly rainfall is 2336 mm $year^{-1}$.

This region, which is located in the Rondonia Juruena Province (Santos et al., 2006; Fig. 1), contains a volcanic basement that is related to the Colider Group (1.78–1.80 Ga). Intruding the volcanic basement are the granitic bodies of the Teodosia (1.758–1.757 Ga) and Igarapé das Lontras (1.754 Ga) suites, all of which are intersected by the monzogranitic batholiths of the Serra da Providência suite (1.57–1.53 Ga, Santos, 2003; CPRM, 2014). Two main basins have developed over the volcanic basement and granitic bodies (Reis et al., 2013; CPRM, 2014): the first was infilled by the rocks of the Sumaúma Supergroup, which comprise a Proterozoic volcano-sedimentary sequence, while the second was infilled by the rocks of the Alto Tapajós Group, which represent a Paleozoic sedimentary sequence (Fig. 1).

According to Reis et al. (2013), the Sumaúma Supergroup is divided in the Vila do Carmo Group and the Beneficente Group. The Vila do Carmo Group (1.76–1.74 Ga) comprises the rift phase of the Sumaúma Supergroup and contains volcanoclastic, pyroclastic and clastic units and quartz-sandstones cut by the Mata-Matá diabase (1.576 Ga) (Betiollo et al., 2009; Reis et al., 2013). The post-rift phase is related to the Beneficente Group (1.43–1.08 Ga), which overlaps the Vila do Carmo Group. The Beneficente Group contains orthoconglomerates and massive quartz-sandstones with rare mudstones deposited in alluvial fans and floodplains; pinkish to purplish silicified quartz-sandstones that were deposited in tidal plains and river channels; and sublitharenites and quartz-sandstones intercalated with siltstones and mudstones that were deposited in aeolian and washover environments (CPRM, 2013; Reis et al., 2013). The Paleozoic basin (i.e., the Alto Tapajós Group) and Cenozoic deposits partially cover the older units.

Weathering has developed iron and aluminous lateritic duricrusts that sustain a strongly dissected landscape formed by plateaus and hills. On the edges of the low dissected plateaus (up to 134 m high) are where the Apuí and Zé Julião Mn deposits crop out (Fig. 2A, B); in the valleys and small hills (20–134 m high) are where the Holanda, Beneficente and Novo Natal Mn deposits crop out (Fig. 2A, B). The analysis of the drainage patterns and relief revealed that all of these Mn deposits are located along NW-SE- and NE-SW-trending structures (Fig. 2A).

3. Materials and methods

In this study, 14 samples collected from five Mn ore deposits were analyzed. Additionally, 21 other samples previously described by Silva et al. (2012) were reevaluated, and new mineralogical and geochemical data for these samples were provided. These deposits were described based on the occurrence, textures, structures and compositions of their minerals. The samples were dried at room temperature, pulverized and submitted to mineral identification using X-ray powder diffraction (Shimadzu XRD – 6000) equipped with a copper tube, as well as scanning electron microscopy (SEM, Quanta 250 FEI) following Au-Pd metallization. The electron microprobe analysis (EMPA, JEOL JXA8230) of polished thin sections provided chemical microanalysis (of SiO_2, Al_2O_3, Fe_2O_3, MgO, CaO, Na_2O, K_2O, MnO_2, P_2O_5, CuO, CoO, BaO, PbO and V_2O_5) after carbon metallization. The OH content represents the result of 100% subtracted by the bulk sum of the elements analyzed.

The bulk-rock geochemical analysis was done at Acmelab, Vancouver, Canada. The concentrations of major and minor elements (SiO_2, Al_2O_3, Fe_2O_3, MgO, CaO, Na_2O, K_2O, TiO_2, P_2O_5 and MnO) were determined using ICP-ES after lithium borate fusion. For the quantification of trace elements (Ag, As, Au, Ba, Bi, Be, Cd, Co, Cr, Cs, Cu, Ga, Hf, Hg, Mo, Nb, Ni, Pb, Rb, Sb, Sc, Se, Sn, Sr, Ta, Tl, Th, U, V, W, Y, Zn, Zr and REE), 0.25 g of each sample was heated in HNO_3, $HClO_4$, and HF until fuming and then taken to dryness. The residue was dissolved in HCl and loaded onto an ICP-MS. The loss of ignition (LOI) was analyzed by gravimetry (heated to 1000 °C).

The quantification of minerals involved stoichiometric calculations (Appendix). The mineral quantification associated with statistical analysis allowed us to relate the mineral assemblage to the trace elements. For statistical analysis, the STATISTICA 9.0 software and principal component analysis method (PCA) were used. Elements that were below detection limit in most samples (i.e., MgO and Na_2O) or that had very homogeneous contents (i.e., K_2O, Ag and V) were not used in this statistical analysis. Geology and relief maps were constructed using ArcGis 10 and Global Mapper 13.

4. Results

4.1. Novo Natal deposit

4.1.1. Pinkish siltstone and Mn-greywackes

At Novo Natal, pinkish siltstones and Mn-greywackes crop out (when Mn-greywackes and pinkish siltstone are discussed together, they are referred to as Mn-rocks). These are interbedded with acid tuffs and sometimes contain multiple quartz geodes that are up to 2 cm in diameter. The pinkish siltstone (sample PS) has a quartz framework (78% of the bulk rock) and displays a brecciated texture associated with a series of NW-SE- and NE-SW-trending fractures (Figs. 3 and 4A). The Mn-minerals that fill fractures and make up 20% of the bulk rock are coronadite (12%), hollandite (6%) and cryptomelane (approximately 2%) (Fig. 7A, Table 1). The quartz framework also contains 2% hematite and goethite (Table 1). Overlapping the pinkish siltstone is a tabular grayish Mn-greywacke (sample A3) that is fine- to medium-grained, contains well-sorted and rounded quartz grains (48%), and is supported by a matrix of romanechite (26%), hollandite (23%) and cryptomelane (1%) that is intersected by millimeter-scale veins of coronadite (1%) (Figs. 3 and 4B, Table 1). Hematite and goethite (~2%; Table 1) fill cavities and pores, while scarce nuggets of Ag (~15 μm) are widespread throughout the matrix (Fig. 8A).

4.1.2. Mn duricrusts

From the pinkish siltstones and Mn-greywackes developed a Mn lateritic duricrust that is up to 3.3 m thick. Laterally, there are some phosphatic portions of the solid solution of crandallite and goyazite (sample Pd) that preserve stratification (Figs. 4C and 7B). The duricrust is massive (sample M1), protopisolitic (samples Pp1 and Pp2) and pisolitic (samples Pi1 and Pi2) (Fig. 3). The massive duricrust has a powdery and friable framework featuring cryptomelane (34%), hollandite (25%) and pyrolusite (24%) intergrown with gibbsite (14%) (Figs. 4D and 7C, Table 1). Fractures and cracks are filled by pinkish and hard

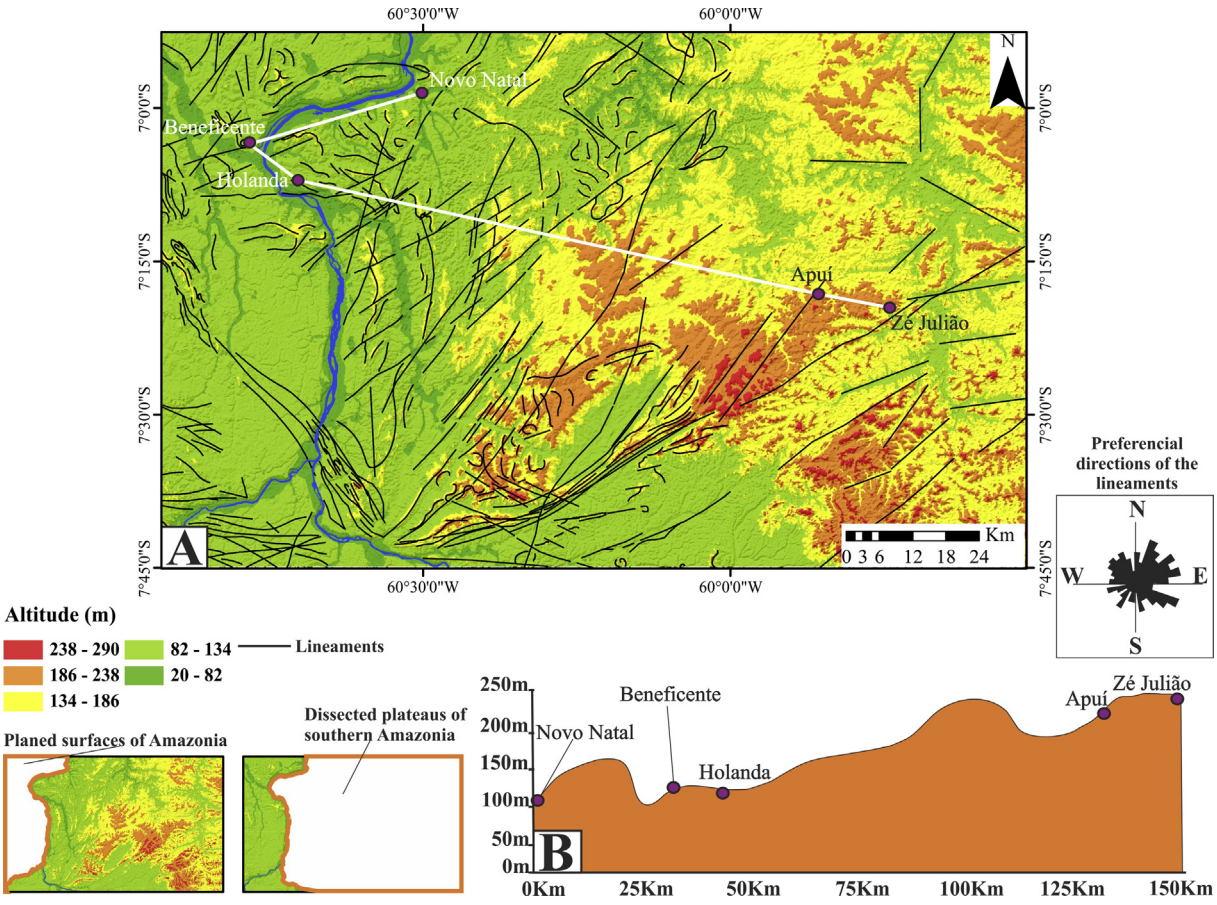

Fig. 2. (A) Planialtimetric map and main tectonic structures. (B) Planialtimetric profile between Novo Natal and Zé Julião deposits.

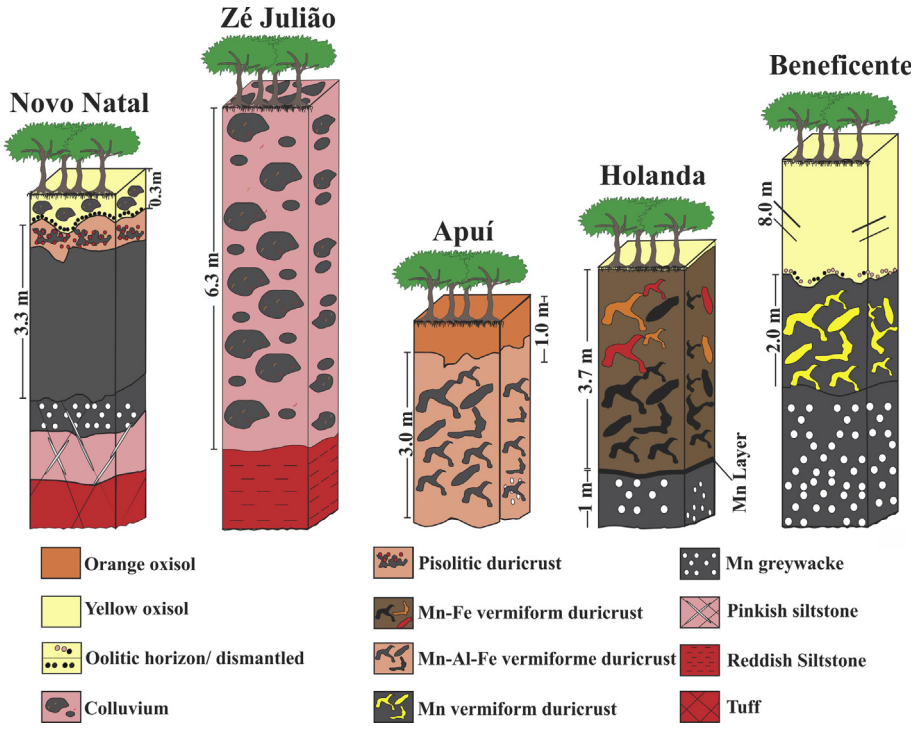

Fig. 3. Schematic profiles of the five studied Mn deposits.

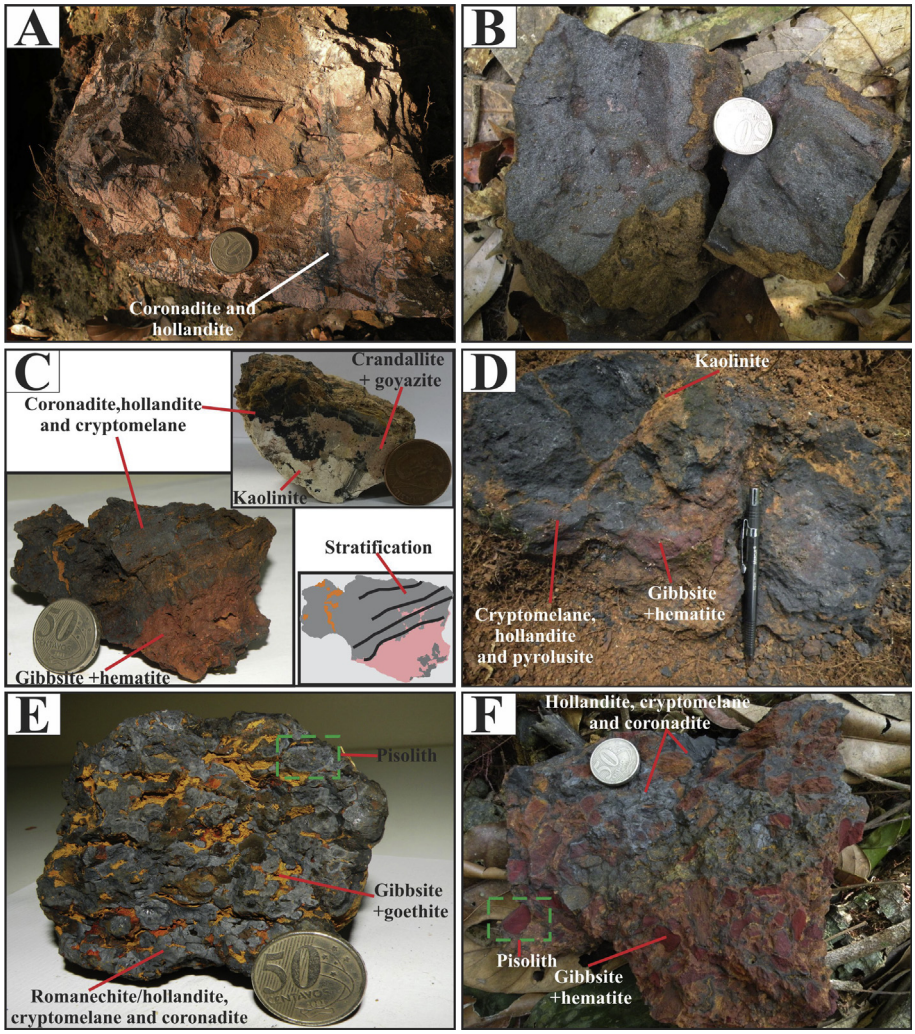

Fig. 4. Macroscopic features of the Novo Natal deposit. (A) Pinkish siltstone (PS) with manganese filling fractures. (B) Tabular Mn-greywacke (A3). (C) Remnant stratification in Mn-duricrusts and phosphorous manganese duricrust of crandallite, goyazite, hollandite, cryptomelane and coronadite. (D) Massive duricrust (M1) with framework composed by cryptomelane, hollandite and pyrolusite and fractures filled by gibbsite, goethite and hematite. (E) Protopisolitic duricrust (Pp1 and Pp2) with romanechite and pyrolusite and cavities filled by goethite and hematite. (F) Pisolitic duricrust (Pi1) showing gibbsitic and hematitic pisoliths enveloped by hollandite, coronadite and cryptomelane plasma.

gibbsite, goethite and hematite. The protopisolitic duricrust is bluish-grey, hard and has submetallic brightness (Fig. 4E). The framework (comprising 60 to 80% of these duricrusts) is composed of cryptomelane (6–14%) and coronadite (1–2%) (Table 1); however, in sample Pp1, the main mineral is hollandite (93%), whereas the main mineral in Pp2 is romanechite (76%) (Fig. 7D, Table 1). The few pisoliths (<1.5 cm in diameter) have tinny cores and frosted cortexes composed of the same minerals as the framework. The cavities (comprising 20–40% of the duricrust) are filled with gibbsite, quartz, kaolinite, goethite and hematite.

The pisolitic duricrust (sample Pi1) has reddish hematite and gibbsite pisoliths (comprising 15–54% of the duricrust) surrounded by pinkish gibbsite (30–40%) and kaolinite (6–15%) plasma (Figs. 3 and 4F, Table 1). Hollandite (29%), cryptomelane (9%) and coronadite (1%) fill voids and fractures (Table 1). In this Mn-plasma, there are tiny and scarce crystals of galena (<10 μm long; Fig. 8B). The upper portion of the pisolitic duricrust (sample Pi2) contains more goethite (27%) and hematite (27%) (Table 1). Close to the surface, the Mn duricrust is dismantled, showing angular rounded fragments and pisoliths in abrupt contact with oxisol. The yellowish sandy clay oxisol (sample S7), which is 0.5 m thick (Fig. 3), is composed of gibbsite, kaolinite, and quartz with subordinate hematite and anatase. Similar material also covers the slopes.

4.2. Zé Julião deposit

4.2.1. Mn colluvium

Colluvium that is up to 6 m thick was developed from the reddish siltstone (Fig. 3). It is formed by angular fragments (up to 0.4 m in diameter) of hollandite (2–32%) and/or romanechite (12–84%), coronadite (2–4%) and cryptomelane (1–5%) (Table 1, Fig. 7E). It has a grayish-blue, dense and hard framework with metallic brightness (Fig. 5A) or a grayish, sandy clay, friable, porous and pulverulent framework with earthy brightness and moderate density (Fig. 5B). As in Novo Natal, tiny and scarce galena crystals occur. Cavities, fractures and fissures that are similar to those of the Mn vermiform duricrust are filled by kaolinite, quartz, gibbsite, goethite and hematite.

4.3. Apuí deposit

4.3.1. Mn duricrusts

In this deposit, only vermiform duricrust (3 m) and oxisol (1 m) outcrop (Fig. 3). At the bottom, the vermiform duricrust (sample VB) has a bluish-brown skeleton, encompasses 54% of the bulk crust, and is composed of cryptomelane, hollandite and coronadite (27%), with minor amounts of goethite and hematite. Filling the

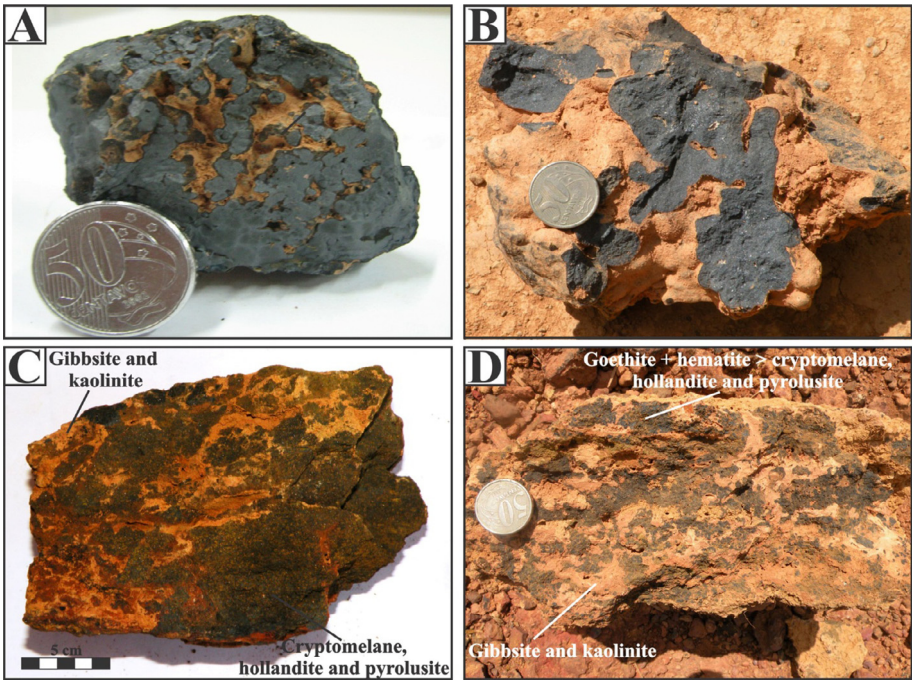

Fig. 5. (A and B) Colluvium fragment of Zé Julião showing metallic brightness and, in detail, the contact among kaolinite and hollandite, coronadite and cryptomelane. (C) Vermiform duricrust of Apuí (VB) with higher content of manganese minerals than gibbsite and kaolinite. (D) Upper part of the vermiform duricrust (VT) showing more goethite and hematite than Mn-minerals (cryptomelane, hollandite and pyrolusite).

skeleton is a pinkish plasma (comprising 46% of the crust) of gibbsite (32%), kaolinite (13%) and rutile (1%) (Table 1). At the top (sample VT), the vermiform duricrust contains more hematite (38%) and goethite (12%) than Mn-minerals (19%) (Fig. 5C and D, Table 1). The orange sandy oxisol (sample S5) is composed of quartz (43%), gibbsite (33%) and kaolinite (8%), as well as loose hematite pisoliths with brown goethite coatings. Tiny crystals of cerianite (CeO_2) and galena that are 3–10 μm long are intergrown with acicular hollandite and gibbsite (Fig. 8C).

4.4. Holanda and Beneficente deposits

4.4.1. Mn-greywackes

These deposits (Fig. 6A and B) are complementary and feature a bedrock of grayish-blue, porous, medium- to coarse-grained Mn-greywacke (samples A1–A2) that is up to 2.5 m thick in outcrops (Figs. 3, 6C, D). The Holanda Mn-greywackes contain several Mn-layers (up to 8 cm thick) of romanechite (77%), pyrolusite (16%) and cryptomelane (3%) that are associated with kaolinite, hematite and goethite (<2%) (Table 1). In both deposits, quartz grains (23% and 33%, respectively) are moderately well- to well-sorted, subrounded to subspherical and often fractured, with evidence of dissolution. The Mn-matrix in both deposits (64–75% of the bulk rock) is composed of romanechite (63–74%) in both its acicular and botryoidal forms (Fig. 7F). Cryptomelane, hematite, goethite and barite (<20 μm long, Fig. 8D) are subordinate minerals (≤2%). In the Mn-greywackes of the Beneficente Group, there is also whitish kaolinite and hollandite and cryptomelane lenses that are up to 6 cm long. Underlying the Mn-greywacke of the Beneficente Group is goethitic sandstone.

4.4.2. Mn duricrusts

From Mn-greywackes were developed lateritic vermiform duricrusts (samples H1 to H4 in Holanda and B1 to B4 in Beneficente) with thicknesses ranging from 2 to 3.7 m (Figs. 3, 6E and F). The skeletons of H1 and H4 are porous, have earthy brightness and are composed of romanechite (35–60% of the bulk rock), cryptomelane (1–2%), kaolinite (15–28%), quartz (6–20%), goethite (8–12%) and hematite (6–7%) (Table 1). The Beneficente duricrust is bluish, hard, has metallic brightness and is composed of romanechite (64–80% of the bulk rock), quartz (12–16%) and occasionally pyrolusite (9–19%), as well as minor amounts of goethite (2–5%) and hematite (1–2%). Toward the top occurs a layer (Pi6) that is 10 cm thick and contains red and orange pisoliths of hematite (34%) and goethite (11%) that are sustained by gibbsite (17%), kaolinite (12%) and traces of pyrolusite (<1%) (Fig. 3; Table 1). Cavities (20%) are filled by kaolinite, goethite and hematite.

Oxisol is thin at Holanda and reaches a thickness of 8 m at Beneficente (sample S6). It is yellowish, rich in quartz and kaolinite, and contains vertical reddish spots that are hard and hematitic (Fig. 3).

5. Geochemistry

5.1. Major and minor elements

Overall, in all samples, the contents of MgO and Na_2O are <0.01% (Table 2). The MnO content in the Mn-rocks ranges between 12.96% and 46.93%, whereas in the Mn-layer of Holanda, it reaches up to 68.95% (Table 2). In most of the duricrusts and colluvium fragments, MnO and Fe_2O_3 are the main elements, although their concentrations are highly variable (13.13–62.66% MnO and 2.17–50.02% Fe_2O_3) due to the diversity in textures (i.e., massive, protopisolitic and pisolitic) that control the mineral content. Near the surface, the contents of Al_2O_3, TiO_2 and LOI increase due to the amounts of gibbsite, kaolinite and anatase/rutile that are present in the duricrusts and oxisols. The contents of P_2O_5 up to 0.81% may be related to the solid solution of crandallite/goyazite (Table 2).

5.2. Trace elements

The Mn-rocks and duricrusts record the highest concentrations of Ba and Co (<205,541 and 2696 ppm, respectively) as well as Pb,

Fig. 6. Macroscopic features of the manganiferous deposits. (A) Galery mine of Beneficente showing Mn-greywaCke, duricrust and oxisol. (B) Holanda outcrop showing the lateral extension of Mn-greywacke and duricrust. (C and D) Mn-greywackes of Holanda (A1) and Beneficente (A2), respectively. (E) Vermiform duricrust overlying the Mn greywacke of Beneficente (B1–B4). (F) Vermiform duricrust (H1–H4) overlying the Mn greywacke of Holanda.

especially in the Mn-rocks of Novo Natal (17,200–43,638 ppm) (Table 3). The concentrations of other elements, such Sr, Cu and Zr, must also be highlighted; Sr and Cu record concentrations of up to 999 and 3579 ppm, respectively, and are more concentrated in the duricrusts and colluvium fragments of Novo Natal and Zé Julião. In contrast, Zr is more concentrated in the upper part of the Beneficente oxisol (1065 ppm) (Table 3).

Relative to the bulk continental crust of Taylor and McLennan (1985), all of the Mn-rocks and duricrusts are enriched in Ag, As, Ba, Co, Mo, Pb and Tl (Fig. 9). However, the Novo Natal deposit is most enriched in Ag, Cu, Pb and Tl (in the duricrust), while Apuí is less enriched in Co (Fig. 9A and C).

The Apuí duricrusts and the Novo Natal oxisol (sample S7) record the highest REE concentrations (491–1402 ppm); the Mn-greywacke (sample A3) records the lowest REE concentrations (Table 4). Relative to chondritic values (Taylor and McLennan, 1985), all samples are enriched in REE and record the depletion of HREE relative to LREE (with La_N/Yb_N ratios of 1-75.81) (Fig. 10). The pinkish siltstones of Novo Natal record negative Eu anomalies ($Eu/Eu^* = 0.38$), while the Zé Julião ($Eu/Eu^* = 1.28–2.08$) and Beneficente duricrusts record positive Eu anomalies ($Eu/Eu^* = 2.5–3.09$). The Beneficente duricrusts also record negative Tb anomalies ($Tb/Tb^* = 0.21–0.79$), the vermiform duricrusts of Apuí record positive Ce anomalies ($Ce/Ce^* = 10.96–26.35$), and the Apuí ($Gd/Gd^* = 1.86–2.15$) and Novo Natal ($Gd/Gd^* = 1.13–1.84$) duricrusts record positive Gd anomalies (Table 4).

5.3. Geochemical associations

Within the entire data set, principal component analysis (PCA) was applied to selected elements with loads of >0.2 (except for K_2O, MgO, Na_2O, Ag and V) and were loaded together with the mineral amounts shown in Table 1. The dataset was better described using factors 1 and 2, which expressed 37.12% and 19.26% of the observed variance, respectively. The previous analysis of chemical features, in addition to their mineralogic distribution, allowed five main groups of samples and their geochemical associations to be recognized: Group 1- pisolitic and vermiform duricrusts of Novo Natal and Apuí (samples Pi1, Pi2, VB and VT), together with most samples of the Zé Julião colluvium (Z4-Z7), contain goethite, hematite, and gibbsite, which are associated with Al_2O_3, Fe_2O_3, LOI, Th, Sc, Rb, Y, U, Ce, Pr, Nd, Ho, Er, Tm and Yb; Group 2- Mn-greywackes and duricrusts of Beneficente and Holanda (except H2) and samples Z1 to Z3 of the Zé Julião colluvium are associated with romanechite, MnO, CaO, Ba, Ni, Be, Co, Zn and Mo; Group 3- Mn-rocks of Novo Natal (samples PS and M3) feature an association defined by quartz, coronadite, SiO_2, P_2O_5 and Pb; Group 4- Mn-layer of Holanda and the massive and protopisolitic

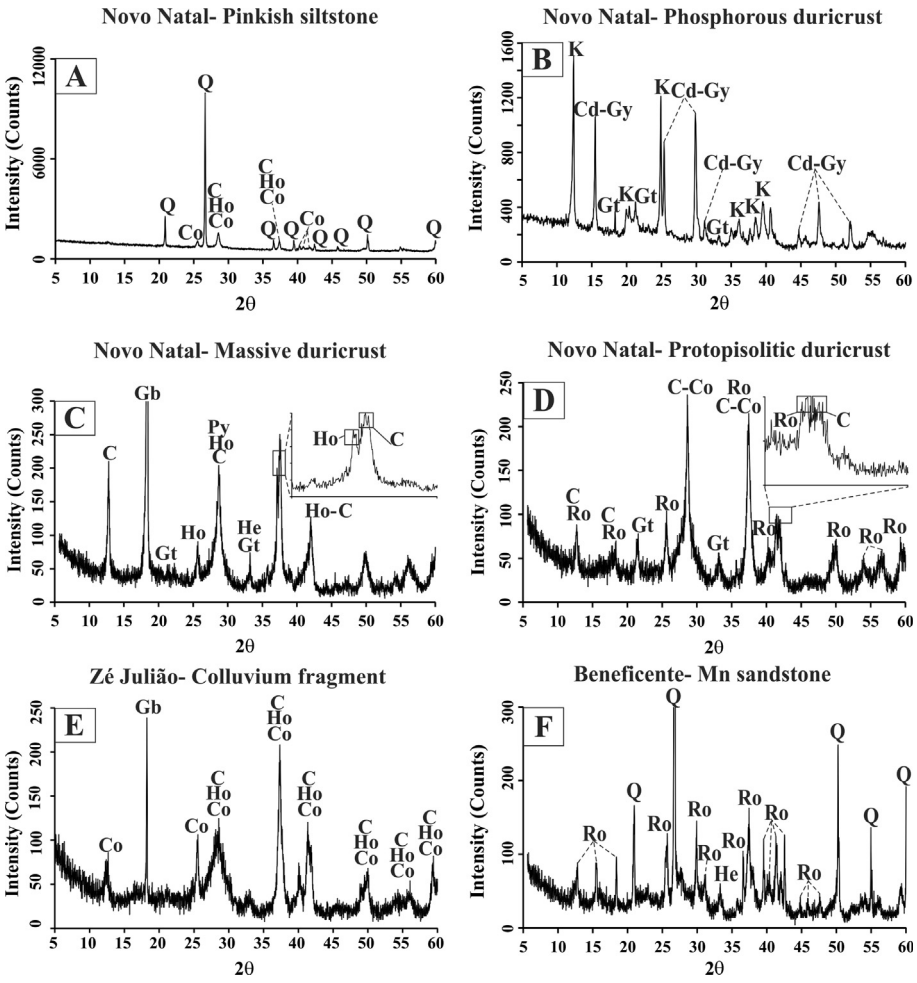

Fig. 7. Mineral most common at the Mn-rocks and related duricrust. C- cryptomelane, Co- coronadite, Cd- crandallite, He- hematite, Ho- hollandite, Gb- gibbsite, Gt- goethite, Gy- goyazite, Py- pyrolusite, Q- quartz and Ro- romanechite.

Table 1
Mineral content in weight%. Q- quartz, C-cryptomelane, Co- coronadite, Ho- hollandite, Ro- romanechie, Py- pyrolusite, Gt- goethite, He- hematite, K- kaolinite, An/Ru- anatase or rutile and Il- illite. – not identified.

Lithotype	Sample	Q	C	Co	Ho	Ro	Py	Gt	He	K	Gb	An/Ru	Il	Sum
Novo Natal														
Oxisol	S7	24	–	–	–	–	–	2	8	26	38	2	–	100
Duricrust	Pi2	–	–	–	–	–	–	27	27	15	30	1	–	100
Duricrust	Pi1	–	9	1	29	–	–	10	5	6	40	<1	–	100
Duricrust	Pp2	–	14	2	–	76	–	5	1	–	2	–	–	100
Duricrust	Pp1	–	6	1	93	–	–	–	–	<1	–	–	–	100
Duricrust	M1	1	34	–	25	–	24	2	<1	–	14	–	–	100
Mn greywacke	A3	48	1	1	23	26	–	<1	1	–	–	–	–	100
Pinkish siltstone	PS	78	2	12	6	–	–	<1	1	–	–	–	–	100
Zé Julião														
Colluvium fragment	Z8	39	1	2	17	–	–	11	13	3	14	<1	–	100
Colluvium fragment	Z7	10	2	3	32	–	–	21	10	<1	22	1	–	100
Colluvium fragment	Z6	14	1	–	–	12	–	16	25	3	28	1	–	100
Colluvium fragment	Z5	–	2	–	–	49	–	11	10	21	6	<1	–	100
Colluvium fragment	Z4	5	3	–	–	52	–	13	9	9	9	<1	–	100
Colluvium fragment	Z3	5	5	4	2	84	–	<1	<1	–	–	<1	–	100
Colluvium fragment	Z2	5	2	–	5	58	–	15	7	–	8	<1	–	100
Colluvium fragment	Z1	5	3	2	19	49	–	12	3	–	7	<1	–	100
Apuí														
Oxisol	S5	43	–	–	–	–	–	<1	14	8	33	1	–	100
Duricrust	VT	–	2	1	15	–	–	12	38	3	28	<1	–	100
Duricrust	VB	–	8	1	18	–	–	11	16	13	32	1	–	100
Holanda														
Duricrust	H4	6	1	–	–	60	–	12	6	15	–	<1	–	100

(*continued on next page*)

Table 1 (*continued*)

Lithotype	Sample	Q	C	Co	Ho	Ro	Py	Gt	He	K	Gb	An/Ru	Il	Sum
Duricrust	H3	10	2	–	–	54	–	8	6	20	–	<1	–	100
Duricrust	H2	20	1	–	–	35	–	9	7	28	–	1	–	100
Duricrust	H1	12	1	–	–	51	–	10	7	19	–	<1	–	100
Mn layer	ML	–	3	–	–	77	16	1	1	2	–	<1	–	100
Mn greywacke	A1	23	1	–	–	74	–	1	1	–	–	<1	–	100
Beneficente														
Oxisol	S6	28	–	–	–	–	–	10	14	47	–	1	–	100
Oxisol	S6	32	–	–	–	–	–	17	12	38	–	1	–	100
Duricrust	Pi6	25	–	–	–	–	<1	11	34	12	17	1	–	100
Duricrust	B4	12	–	–	–	72	9	5	2	–	–	–	–	100
Duricrust	B3	14	–	–	–	64	19	2	1	–	–	–	–	100
Duricrust	B2	12	1	–	–	84	–	2	1	–	–	–	–	100
Duricrust	B1	16	–	–	–	80	–	3	1	–	–	–	–	100
Mn greywacke	A2	33	1	–	–	63	–	2	1	–	–	–	–	100

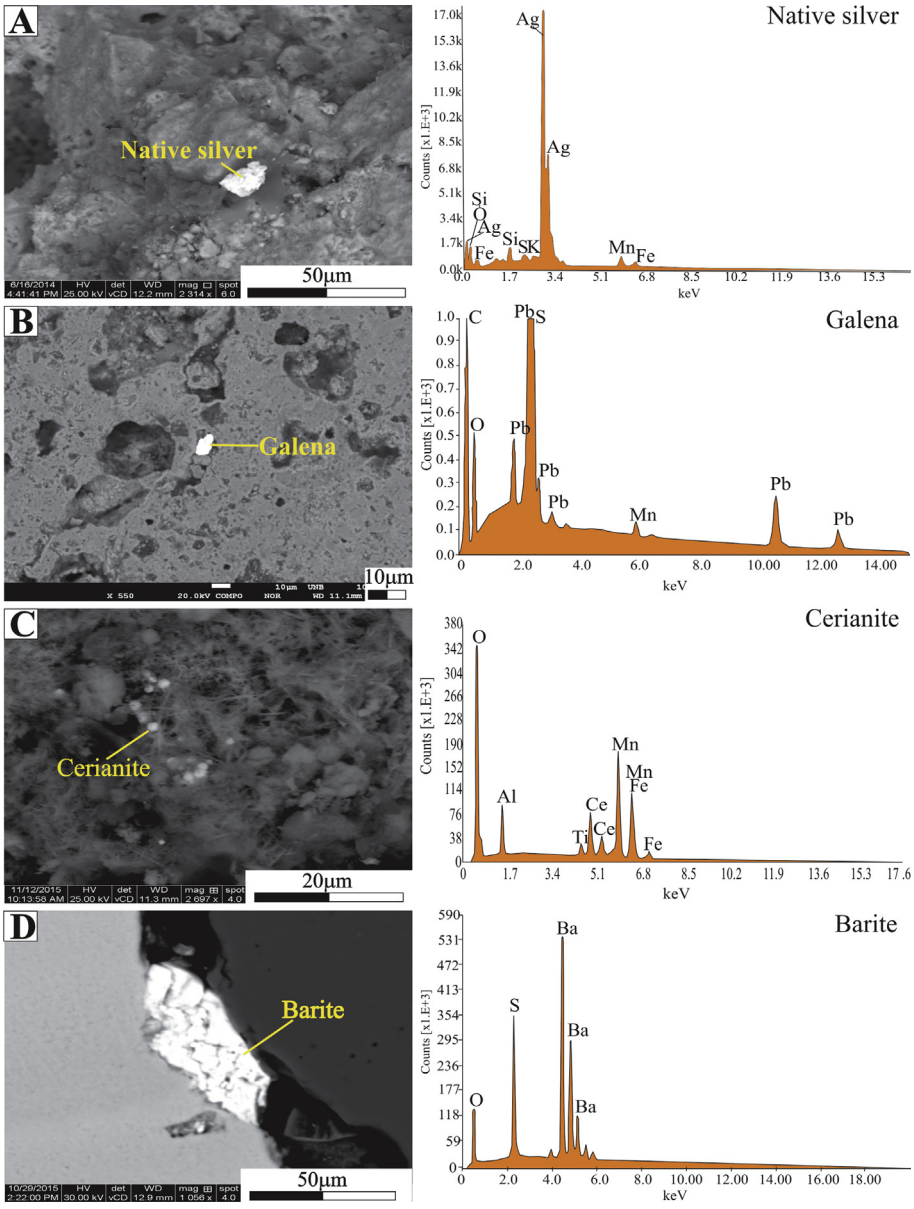

Fig. 8. (A) Native silver found in the Mn-greywacke (A3) of Novo Natal and respective EDS. (B) Tiny crystal of galena in the pisolitic duricrust (Pi1) of the Novo Natal and respective. (C) Tiny crystals of cerianite in vermiform duricrust of Apuí and respective EDS. (D) Tiny crystal of barite found in Mn-greywacke (A2) of Beneficente and respective EDS.

Table 2
Chemical composition (wt%). *Sum not closer to 100% is due to high contents of Ba and Pb.

Lithotype	Sample	SiO_2	Al_2O_3	Fe_2O_3	K_2O	CaO	MgO	MnO	Na_2O	P_2O_5	TiO_2	LOI	Sum
Novo Natal													
Oxisol	S7	34.59	33.83	9.94	0.05	0.01	0.01	0.57	<0.01	0.26	1.51	18.6	99.37
Duricrust	Pi2	6.06	22.54	48.37	0.01	0.02	<0.01	4.83	<0.01	0.10	0.88	16.7	99.51
Duricrust	Pi1	2.40	27.87	15.68	0.52	0.09	<0.01	25.82	0.02	0.32	0.47	19.8	92.99
Duricrust	Pp2	0.23	1.00	5.33	0.73	0.14	<0.01	54.1	0.02	0.31	0.09	11.7	73.65
Duricrust	Pp1	0.68	1.10	5.95	0.34	0.11	<0.01	53.11	0.01	0.35	0.06	11.4	73.11
Duricrust	M1	0.72	8.42	5.28	2.13	0.03	<0.01	62.66	0.07	0.13	0.04	14.9	94.38
Mn greywacke	A3	46.70	0.70	3.30	0.07	0.06	<0.01	32.82	<0.01	0.24	0.02	6.1	90.01
Pinkish siltstone	PS	73.39	1.91	2.00	0.15	0.02	<0.01	12.96	<0.01	0.34	0.05	3.2	94.02
Zé Julião													
Colluvium	Z8	39.43	10.00	25.03	0.06	0.02	<0.01	11.27	<0.01	0.31	0.43	10.5	97.05
Colluvium	Z7	10.12	14.23	33.88	0.11	0.03	<0.01	20.69	<0.01	0.41	0.49	15.1	95.06
Colluvium	Z6	14.88	18.80	40.28	0.07	0.02	<0.01	8.32	<0.01	0.16	0.72	14.7	97.95
Colluvium	Z5	10.58	12.66	20.63	0.16	0.05	<0.01	32.95	<0.01	0.33	0.50	13.2	91.06
Colluvium	Z4	9.33	10.88	21.30	0.22	0.07	<0.01	34.86	0.01	0.37	0.47	13.2	90.71
Colluvium	Z3	5.14	3.80	9.76	0.25	0.09	<0.01	47.9	0.01	0.43	0.18	11.5	79.06
Colluvium	Z2	5.28	4.33	18.74	0.14	0.06	<0.01	45.8	<0.01	0.55	0.29	12.0	87.19
Colluvium	Z1	4.95	4.21	14.46	0.18	0.05	<0.01	49.58	<0.01	0.55	0.35	12.7	87.03
Apuí													
Oxisol	S5	46.66	24.93	13.80	0.12	0.01	0.04	0.10	<0.01	0.03	1.14	12.9	99.73
Duricrust	VT	1.64	19.35	50.02	0.14	0.03	<0.01	13.13	0.01	0.15	0.28	12.7	97.45
Duricrust	VB	5.81	25.20	28.34	0.54	0.10	<0.01	20.70	0.03	0.16	0.55	17.0	98.43
Holanda													
Duricrust	H4	14.22	5.99	18.21	0.07	0.2	<0.01	38.88	<0.01	0.42	0.28	11.9	90.17
Duricrust	H3	19.56	7.80	14.33	0.13	0.06	<0.01	35.86	<0.01	0.34	0.36	11.5	89.94
Duricrust	H2	33.19	10.93	15.58	0.08	0.02	<0.01	22.51	<0.01	0.35	0.56	10.7	93.92
Duricrust	H1	21.38	7.68	17.52	0.04	0.05	<0.01	32.38	<0.01	0.44	0.46	11.5	91.45
Mn layer	ML	0.75	0.77	1.54	0.17	0.11	<0.01	68.95	0.01	0.41	0.03	11.2	83.94
Mn greywacke	A1	23.59	5.81	1.37	0.07	0.06	<0.01	46.93	<0.01	0.27	0.22	10.6	88.92
Beneficente													
Oxisol	S6	46.42	18.27	22.66	0.01	0.02	<0.01	0.05	<0.01	0.75	1.04	10.6	99.82
Oxisol	S6	46.54	14.07	26.42	<0.01	0.02	<0.01	0.05	<0.01	0.81	0.78	11.2	99.89
Duricrust	Pi6	33.10	13.97	40.92	0.02	0.01	<0.01	0.53	<0.01	0.54	0.73	9.1	98.92
Duricrust	B4	10.88	2.80	6.09	0.07	0.07	<0.01	54.49	<0.01	0.77	0.19	10.7	86.06
Duricrust	B3	12.73	1.73	2.83	0.07	0.06	<0.01	58.99	<0.01	0.43	0.15	9.9	86.89
Duricrust	B2	10.48	1.18	2.17	0.05	0.05	<0.01	55.55	<0.01	0.35	0.09	9.3	79.22
Duricrust	B1	14.60	1.62	3.41	0.04	0.05	<0.01	55.95	<0.01	0.40	0.11	9.8	85.98
Mn greywacke	A2	25.33	1.35	2.28	0.06	0.09	<0.01	39.55	<0.01	0.71	0.08	9.1	78.55

Table 3
Trace elements concentrations (ppm).

Lithotype	Sample	Ag	As	Ba	Be	Co	Cu	Ga	Hf	Mo	Nb	Ni	Pb	Rb	Sc	Sr	Tl	Th	U	V	Y	Zr	Zn
Novo Natal																							
Oxisol	S7	1	51	1713	<1	46	166	48	29	4	45	8	401	2	23	61	1	39	10	61	104	1065	10
Duricrust	Pi2	1	95	612	3	259	261	70	15	19	21	17	495	7	28	45	8	51	5	535	28	545	23
Duricrust	Pi1	19	142	44690	9	878	2702	63	11	27	5	48	14100	11	11	610	62	15	5	119	22	452	246
Duricrust	Pp2	25	80	99500	21	1786	3579	117	4	66	3	57	4391	7	5	990	97	20	11	90	66	119	248
Duricrust	Pp1	20	64	120300	21	1918	3412	122	2	90	2	52	292	5	4	507	58	5	10	107	54	52	224
Duricrust	M1	84	76	44794	7	1036	1643	96	1	24	<0.1	27	5001	21	5	168	45	2	5	65	26	47	148
Mn greywacke	A3	5	75	71100	2	522	2016	63	1	57	2	13	17200	2	3	51	7	2	5	80	5	32	117
Pinkish siltstone	PS	2	40	14055	6	359	1446	14	2	27	1	10	43638	4	2	19	2	1	2	<8	5	16	38
Zé Julião																							
Colluvium	Z8	1	79	20413	8	453	386	38	12	10	10	57	529	2	16	51	5	39	6	284	18	389	88
Colluvium	Z7	2	137	33348	10	782	566	51	14	11	12	72	238	2	40	103	10	40	12	467	26	490	130
Colluvium	Z6	1	30	14632	4	318	330	71	10	6	18	26	169	1	38	59	5	39	8	668	20	357	66
Colluvium	Z5	2	27	85230	12	1203	743	60	11	11	8	43	197	2	34	328	17	31	9	508	27	412	165
Colluvium	Z4	2	43	88741	15	1236	713	62	10	12	8	63	185	3	30	390	15	27	11	479	27	354	185
Colluvium	Z3	2	41	204315	21	1941	1333	72	4	20	3	71	109	4	24	580	25	10	13	260	18	130	228
Colluvium	Z2	2	53	122954	19	1713	754	89	7	23	7	82	368	5	26	999	19	16	12	249	25	254	199
Colluvium	Z1	2	37	125533	20	1603	855	87	10	21	7	81	244	6	23	131	16	16	13	215	25	332	196
Apuí																							
Oxisol	S5	<0.1	3	105	<1	4.6	2	36	17.2	0.8	27	5.3	10	7	13	51	<0.1	30	4	131	42	594	5
Duricrust	VT	1	23	9541	4	254	11	66	6.0	3.0	12	56	2180	14	19	95	8	22	6	144	20	223	81
Duricrust	VB	1	21	19954	11	389	80	40	3.5	3.3	7	90	1141	13	11	39	5	13	5	149	11	125	165
Holanda																							
Duricrust	H4	0.8	44	96627	14	446	24	64	7	4	6	47	23	3	16	95	9	10	4	229	15	242	153
Duricrust	H3	0.6	34	97619	14	1047	20	63	8	9	7	64	50	6	15	102	19	17	7	674	21	296	213
Duricrust	H2	0.4	32	47531	7	669	16	40	12	5	12	42	40	5	18	31	15	16	6	608	18	416	208

(*continued on next page*)

Table 3 (*continued*)

Lithotype	Sample	Ag	As	Ba	Be	Co	Cu	Ga	Hf	Mo	Nb	Ni	Pb	Rb	Sc	Sr	Tl	Th	U	V	Y	Zr	Zn
Duricrust	H1	0.6	30	82187	17	1290	21	62	9	6	11	39	28	2	19	47	10	12	5	749	19	344	270
Mn layer	ML	0.3	12	155748	21	2696	53	69	1	17	1	188	12	4	3	125	23	1	4	522	39	18	712
Mn greywacke	A1	0.4	10	107479	22	1756	28	63	5	9	3	60	10	3	12	67	11	7	5	427	20	169	274
Beneficente																							
Oxisol	S6	<0.1	41	768	1	2	9	45	16	4	19	6	7	0.3	19	42	<0.1	16	11	328	20	584	5
Oxisol	S6	<0.1	29	1038	1	2	8	37	20	2	25	3	10	0.2	19	57	<0.1	21	11	233	26	733	4
Duricrust	Pi6	1	26	1536	1	15	9	46	15	4	17	12	39	1	22	82	0.2	29	9	445	22	547	9
Duricrust	B4	2	86	136475	12	1266	51	61	7	26	4	62	43	1	9	74	13	5	5	478	24	240	258
Duricrust	B3	2	115	128400	13	1310	31	57	4	30	3	112	27	1	5	47	25	4	5	363	10	158	320
Duricrust	B2	2	84	205341	10	1356	32	66	3	25	2	84	16	1	4	32	19	2	2	268	9	95	296
Duricrust	B1	2	102	137727	12	1331	35	61	3	26	3	106	15	1	5	37	16	3	3	242	10	102	298
Mn greywacke	A2	5	102	111200	14	842	78	105	3	28	2	110	67	2	6	64	21	3	4	119	18	104	320
C. Crust	C.C	0.1	2	550	3	17	25	17	5.8	1.5	12	44	17	112	13.6	350	1	11	3	107	22	190	71

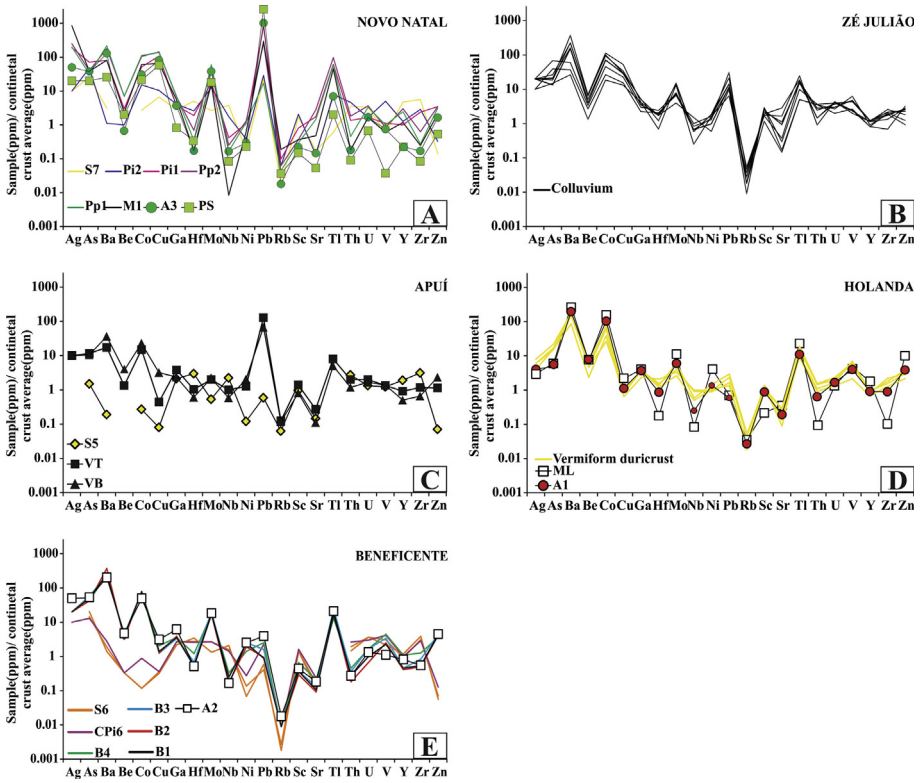

Fig. 9. Trace elements in ppm normalized by the average crustal of Taylor and McLennan (1985).

Table 4
Rare earth elements concentrations (ppm). $Eu/Eu^* = (Eu/0.087)/[(Sm/0.231)\times(Gd/0.306)]^{1/2}$; $Ce/Ce^* = (Ce/0.957)/[(La/0.367)\times(Pr/0.137)]^{1/2}$; $Tb/Tb^* = (Tb/0.06)/[(Gd/0.31)\times(Dy/0.38)]^{1/2}$; $Gd/Gd^* = (Gd/0.31)/[(Eu/0.087)\times(Tb/0.06)]^{1/2}$.

Lithotype	Sample	La	Ce	Pr	Nd	Sm	Eu	Gd	Tb	Dy	Ho	Er	Tm	Yb	Lu	REE	Eu/Eu^*	Ce/Ce^*	Tb/Tb^*	Gd/Gd^*	$(La/Yb)_N$
Novo Natal																					
Oxisol	S7	99.3	207.2	19.46	75.3	15.99	3.1	17.0	3.06	19.07	3.79	11.55	1.85	11.96	1.97	491	0.58	1.10	0.97	1.30	5.61
Duricrust	Pi2	79.4	147.7	14.80	49.2	7.10	1.3	6.0	1.00	5.20	1.00	3.30	0.50	3.40	0.60	321	0.61	1.01	1.02	1.25	15.78
Duricrust	Pi1	61.0	120.5	14.80	55.6	7.50	1.7	6.4	0.80	4.00	0.80	2.20	0.40	2.40	0.40	279	0.75	0.94	0.90	1.30	17.17
Duricrust	Pp2	20.1	65.1	11.80	69.2	25.40	5.9	26.0	4.00	19.50	3.00	8.00	1.10	6.90	1.00	267	0.70	0.99	1.02	1.27	1.97
Duricrust	Pp1	9.3	19.3	3.70	21.9	10.00	2.8	17.4	2.90	15.10	2.80	6.50	1.00	6.00	0.80	120	0.65	0.77	1.02	1.45	1.05
Duricrust	M1	20.8	141.5	13.60	69.8	26.70	5.5	20.3	3.30	14.00	2.20	5.20	0.80	5.00	0.70	329	0.72	1.97	1.12	1.13	2.81
Mn greywacke	A3	7.7	14.0	1.40	6.1	1.30	0.9	8.2	1.20	5.50	1.00	2.70	0.40	2.40	0.30	53	0.84	1.00	1.02	1.87	2.17
Pinkish siltstone	PS	46.0	69.8	9.31	28.1	3.51	0.4	2.2	0.23	1.08	0.17	0.47	0.06	0.41	0.05	162	0.38	0.79	0.85	1.84	75.81
Zé Julião																					
Colluvium	Z8	47.5	121.5	11.43	39.9	7.10	1.31	5.09	0.78	4.11	0.70	2.06	0.36	2.26	0.36	244	0.67	1.22	0.98	1.19	14.20
Colluvium	Z7	33.9	203.9	8.43	29.7	6.05	1.25	5.30	1.00	5.85	1.13	3.34	0.55	3.56	0.54	305	0.67	2.83	1.03	1.12	6.43

Table 4 (*continued*)

Lithotype	Sample	La	Ce	Pr	Nd	Sm	Eu	Gd	Tb	Dy	Ho	Er	Tm	Yb	Lu	REE	Eu/Eu*	Ce/Ce*	Tb/Tb*	Gd/Gd*	$(La/Yb)_N$
Colluvium	Z6	34.8	100.5	7.34	26.0	4.84	1.12	4.26	0.75	4.68	0.88	2.76	0.45	2.99	0.48	192	0.75	1.47	0.96	1.10	7.86
Colluvium	Z5	31.1	227.6	7.71	27.1	5.56	1.35	5.31	1.04	6.49	1.11	3.38	0.54	3.45	0.53	322	0.76	3.44	1.01	1.06	6.09
Colluvium	Z4	40.3	172.7	10.60	37.1	7.47	1.15	6.28	1.13	6.73	1.14	3.38	0.55	3.36	0.50	292	0.51	1.96	0.99	1.31	8.10
Colluvium	Z3	18.8	110.9	5.37	20.8	4.54	3.24	4.98	0.74	5.31	0.68	1.91	0.31	1.83	0.26	180	2.08	2.59	0.82	0.76	6.94
Colluvium	Z2	31.0	128.3	7.95	29.0	6.27	3.15	5.87	0.99	6.90	0.99	2.93	0.46	3.01	0.42	227	1.59	1.91	0.89	0.79	6.96
Colluvium	Z1	34.8	122.8	8.75	32.7	6.58	2.63	5.99	0.95	7.10	0.94	2.90	0.44	2.93	0.42	230	1.28	1.65	0.83	0.90	8.03
Apuí																					
Oxisol	S5	57.6	86	8.23	20.9	4.16	0.86	5.04	1.03	7.18	1.52	4.49	0.73	5.1	0.74	204	0.57	0.92	0.97	1.27	7.63
Duricrust	VT	21.6	451	4.30	16.4	2.9	0.60	4.30	0.50	2.70	0.60	1.60	0.30	1.9	0.30	509	0.52	10.96	0.84	1.86	7.68
Duricrust	VB	25.8	1328	5.40	19.2	3.6	0.80	6.80	0.70	4.50	1.00	2.80	0.50	3.0	0.50	1402	0.49	26.35	0.72	2.15	5.81
Holanda																					
Duricrust	H4	25.1	246.1	6.84	23.0	4.89	1.52	4.03	0.73	4.92	0.75	2.55	0.40	2.59	0.40	324	1.05	4.40	0.94	0.91	6.55
Duricrust	H3	30.5	104.3	7.29	23.7	4.40	0.77	3.40	0.61	4.12	0.71	2.14	0.38	2.45	0.39	185	0.61	1.64	0.93	1.18	8.41
Duricrust	H2	40.9	173.5	11.43	41.5	7.70	1.70	5.76	0.93	6.42	0.90	2.83	0.44	2.84	0.43	297	0.78	1.88	0.87	1.09	9.73
Duricrust	H1	20.1	148.6	7.06	24.5	5.20	1.47	3.71	0.62	4.59	0.59	1.85	0.29	1.94	0.28	221	1.02	2.92	0.86	0.92	7.00
Mn layer	ML	32.8	126.0	18.95	82.7	18.19	4.92	16.09	2.12	14.70	2.15	5.78	0.86	5.25	0.70	331	0.88	1.18	0.79	1.18	4.22
Mn greywacke	A1	36.9	247.5	10.74	38.2	7.74	2.05	5.88	0.89	5.90	0.80	2.33	0.37	2.23	0.33	362	0.93	2.91	0.86	1.03	11.18
Beneficente																					
Oxisol	S6	49.7	101.4	11.87	42.4	7.32	1.35	5.80	0.93	4.97	1.00	2.97	0.53	3.73	0.60	235	0.63	0.98	0.99	1.23	9.00
Oxisol	S6	37.7	76.8	8.95	31.9	5.50	1.04	4.54	0.73	3.96	0.75	2.20	0.41	2.76	0.46	178	0.64	0.98	0.98	1.24	9.23
Duricrust	Pi6	52.9	110.4	12.90	45.9	7.09	1.31	5.13	0.80	4.28	0.87	2.58	0.45	3.20	0.52	248	0.66	0.99	0.98	1.19	11.17
Duricrust	B4	10.0	20.5	3.25	15.0	3.34	2.88	2.43	0.11	2.81	0.30	1.15	0.21	1.09	0.19	63	3.09	0.84	0.24	1.02	6.20
Duricrust	B3	8.1	18.3	2.94	13.8	2.77	1.97	2.05	0.09	2.89	0.30	1.02	0.18	0.94	0.16	56	2.53	0.88	0.21	1.15	5.82
Duricrust	B2	10.8	23.0	2.69	10.9	2.34	2.00	2.19	0.17	4.02	0.53	1.60	0.27	1.62	0.22	62	2.70	1.00	0.33	0.89	4.50
Duricrust	B1	23.4	76.5	10.53	48.2	9.83	3.69	10.29	1.28	8.33	0.96	2.60	0.45	2.91	0.54	200	1.12	1.14	0.79	1.12	5.43
Mn greywacke	A2	15.8	45.2	4.30	17.0	3.40	0.90	2.80	0.40	1.40	0.20	0.60	0.10	0.50	0.10	93	0.89	1.28	1.16	1.11	21.35
Chondrite	CH	0.37	0.96	0.14	0.71	0.23	0.09	0.31	0.06	0.38	0.09	0.25	0.04	0.25	0.04	4	1	1.03	0.99	1	1

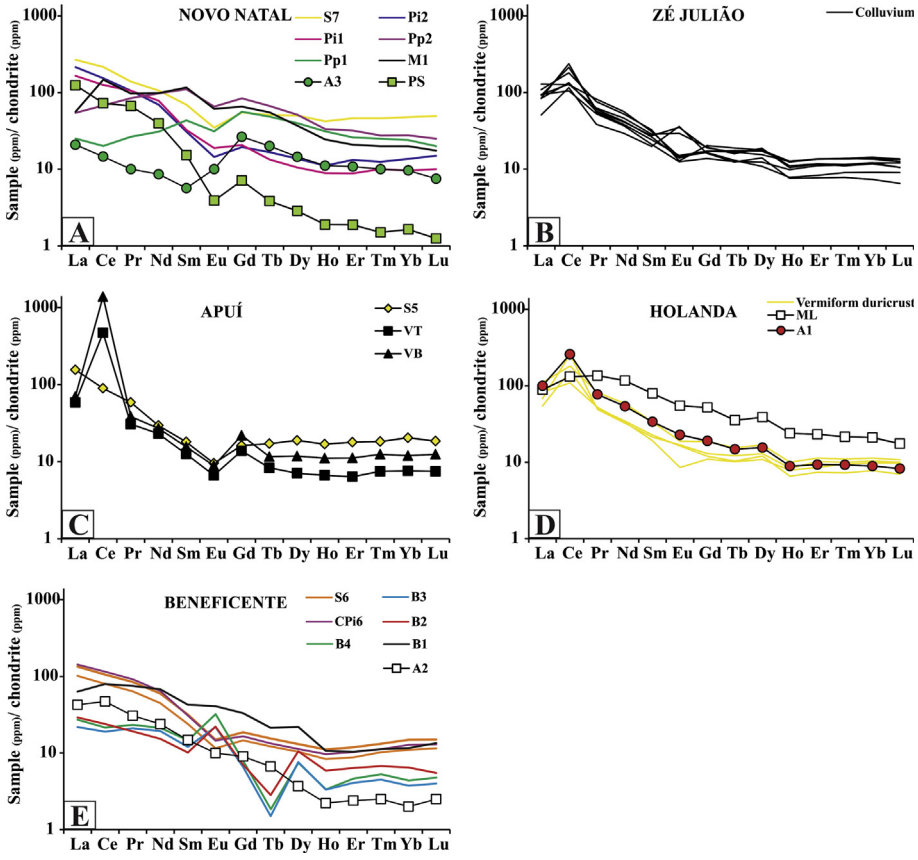

Fig. 10. Rare earth elements in ppm normalized by the chondrite of Taylor and McLennan (1985).

duricrusts of Novo Natal comprise an association of hollandite, cryptomelane, pyrolusite, Ag, As, Cu, Ga, Sr, Tl, Sm, Eu, Gd, Tb and Dy; Group 5- the pisolitic duricrust of Beneficente (sample Pi6), oxisols, the upper portion of the Zé Julião colluvium (sample Z8) and one sample of the vermiform duricrust of Holanda (sample H2) are characterized by the association of kaolinite, anatase/rutile, TiO_2, Zr, Hf, La and Nb (Fig. 11).

6. SEM and EMPA: petrographic and microchemical analysis

6.1. Novo Natal- coronadite and hollandite of Mn-rocks

Coronadite and hollandite fill fractures and veins and display zoned acicular structures. Coronadite generally occupies the inner regions of veins and hollandite occupies the edges of veins; these comprise at least three generations, according to the arrangement of these fractures (Fig. 12A). Coronadite also occurs as rod cells around the quartzose framework of the pinkish siltstone. In the Mn-greywackes, hollandite composes the matrix, while coronadite occurs as veinlets or crystals or is disseminated in the matrix and frequently occurs as crowns around hollandite (Fig. 12B and C). Hollandite also fills fractures or exhibits acicular textures in these Mn-rocks (PS and M3).

6.1.1. Novo Natal, Zé Julião and Apuí lateritic duricrusts and colluvium- hollandite

In the duricrusts of Novo Natal and Apui, hollandite is zoned and shows staghorn and boxwork habits or forms angular fragments. The protopisolitic duricrusts of Novo Natal (Pp1 and Pp2) contain two generations of hollandite: the first one, which is widespread throughout the framework, forms angular fragments (~600 μm in diameter) that encompass less than 2% of the duricrust (Fig. 12D). The second and main generation comprises up to 90% of the duricrust and is zoned, includes angular fragments and is intersected by three generations of hollandite veinlets (Fig. 12D), some of which are Pb-hollandite (that are not related to the hierarchy of the generations of the veinlets), as in the duricrusts and colluvium fragments of Novo Natal and Zé Julião. The angular fragments of hollandite intergrown with gibbsite with staghorn and boxwork habits (Fig. 12E, F and G) are characteristic of the massive and vermiform duricrusts of Novo Natal (M1) and Apuí (VB and VT). Voids are filled by acicular hollandite.

6.2. Mineral geochemistry: coronadite and hollandite: sedimentary rock and duricrust

Coronadite records PbO contents ranging between 16.57 and 28.88% and small amounts of BaO (0.30–8.09%) (Table A4; Fig. 13A). The coronadite in the vermiform duricrusts of Apuí (samples VB and VT) has higher contents of CoO (1.28–1.54%) and lower contents of MnO_2 (60.07–60.48%) compared to those of the Mn-rocks of Novo Natal (samples PS and A3; Table A4). According to formula units based on 16 oxygens and Mn^{4+}/Mn^{2+} calculated assuming full site occupancy, the coronadite in the studied Mn-rocks has the following formula: $Pb_{(0.77-1.24)}Ba_{(0.02-0.37)}Mn^{4+}_{(6.85-6.92)}Mn^{2+}_{(0.59-0.72)}Fe^{3+}_{(0.01-0.02)}Al^{3+}_{(0.11-0.21)}Cu_{(0.06-0.11)}Co_{(0.01-0.03)}V_{(0-0.02)}O_{16}$ (Table A5). In contrast, the coronadite found in the Apuí duricrusts has the following formula: $Pb_{(0.93-1.11)}Ba_{(0.14-0.19)}Mn^{4+}_{(6.40-6.43)}Mn^{2+}_{(0.59-0.65)}Fe^{3+}_{(0.47-0.50)}Al^{3+}_{(0.19-0.27)}Cu_{(0.06-0.1)}Co_{(0.17-0.20)}V_{(0-0.01)}O_{16}$ (Table A5).

In Mn-rocks and duricrusts, hollandite has higher contents of BaO (6.17–17.61%) and MnO_2 (63.71–82.12%) and lower contents of SiO_2, K_2O, CaO, Na_2O, P_2O_5 and V_2O_5 (<1%). Nevertheless, in the protopisolitic (sample Pp2) and phosphatic (Pd) duricrusts of Novo Natal, the K_2O content of the hollandite is higher (<2.1%) (Table A6). Two types of hollandite were identified: the most common contains PbO (0.84–9.42%), whereas the hollandite without PbO only occurs in the protopisolitic duricrust (sample Pp2; Fig. 13A). The hollandite of the vermiform duricrusts (samples VB and VT) of Apui and that of the phosphatic portions (sample Pd) of Novo Natal contain more Al_2O_3 and Fe_2O_3 than the Mn-rocks, although in the Mn-greywacke (sample A3), Fe_2O_3 is higher (<9%). Furthermore, the hollandite from the phosphatic portions (sample Pd) is enriched in P_2O_5, CuO and CoO (Table A6) relative to those in the Mn-rocks. The hollandite of the fragments of Zé Julião colluvium records the highest contents of PbO (5.99–9.42%). According to all of these chemical characteristics and the formula units based on 16 oxygens and Mn^{4+}/Mn^{2+} calculated assuming full site occupancy, the hollandite of the studied Mn-rocks has the following formula: $Ba_{(0.72-0.98)}K_{(0-0.12)}Pb_{(0.05-0.23)}Na_{(0.01)}Mn^{4+}_{(6.64-7.15)}Mn^{3+}_{(0.37-0.40)}Fe^{3+}_{(0.01-0.68)}Cu_{(0.04-0.08)}Co_{(0.01-0.04)}Al^{3+}_{(0.04-0.13)}Si_{(0.01-0.07)}O_{16}$. In contrast, the hollandite in the duricrust has the following formula: $Ba_{(0.34-0.92)}K_{(0-0.37)}Pb_{(0-0.4)}Na_{(0-0.04)}Mn^{4+}_{(6.26-7.32)}Mn^{3+}_{(0.35-0.41)}Fe^{3+}_{(0.01-0.49)}Cu_{(0.06-0.17)}Co_{(0.01-0.10)}Al^{3+}_{(0.04-0.96)}Si_{(0.01-0.17)}O_{16}$ (Table A7).

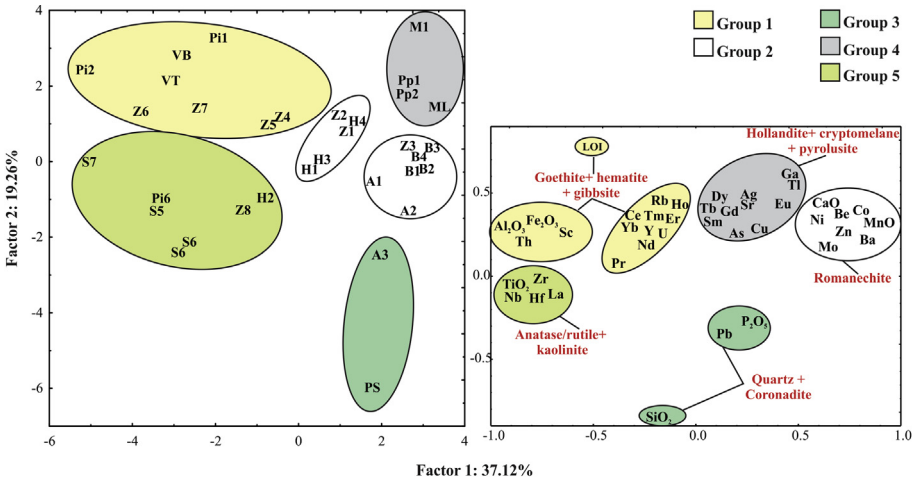

Fig. 11. The main mineral and geochemical associations that identify the studied lithotypes. A1, A2 and A3: Mn-greywackes of Holanda, Beneficente and Novo Natal. H1–H4: vermiform duricrusts of Holanda. Z1–Z8: colluvium fragments of Zé Julião. B1–B4: vermiform duricrusts of Beneficente. VT and VB: vermiform duricrusts of Apuí. Pi1 and Pi2: pisolitic duricrusts of Novo Natal. Pi6: pisolitic duricrust of Beneficente. M1: massive duricrust of Novo Natal. Pp1 and Pp2: protopisolitic duricrust of Novo Natal. PS: pinkish siltstone. ML: manganiferous layer of Holanda. S6, S7 and S5: oxisols of Beneficente, Novo Natal and Apuí, respectively.

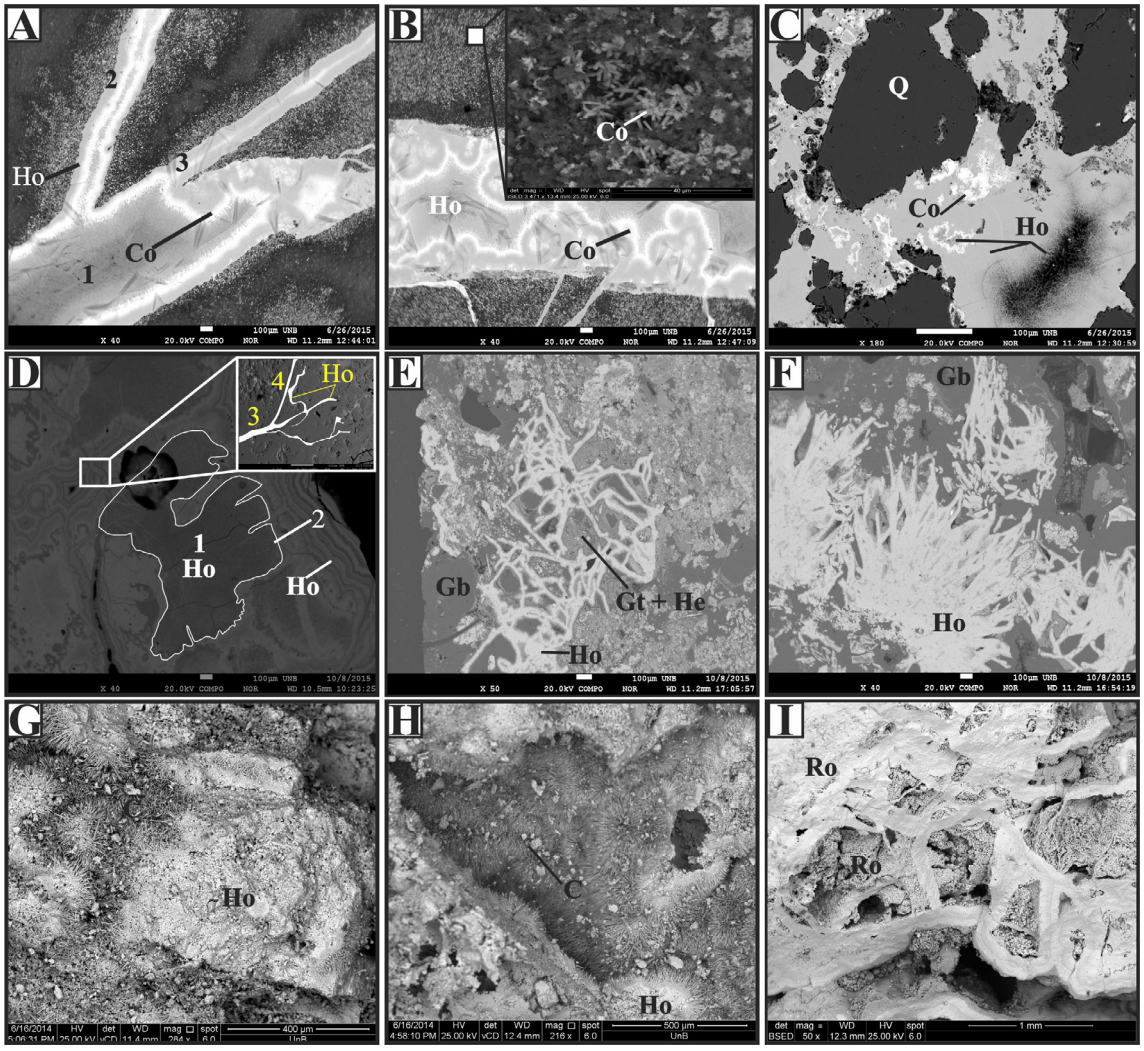

Fig. 12. The main features of the Mn-minerals observed by SEM and EMPA. (A) Fractures of the pinkish siltstone (PS) filled by coronadite (Co) and hollandite (Ho); note the formation of at least three generations of coronadite (1, 2 and 3) and hollandite. (B) Zoned structure displayed by coronadite and hollandite in the pinkish siltstone; into detail the rod cells of coronadite in quartz matrix. (C) Hollandite matrixing quartz (Q) grains of the Mn greywacke (A3), locally it occurs as needles and surrounded by coronadite. (D) Framework of the protopisolitic duricrust (Pp1) composed by at least four generations of hollandite as angular fragments, zoned and veinlets. (E) Relicts of hollandite in the vermiform duricrust of Apuí (VT); note the replamatrix of hollandite for goethite (Gt), hematite (He) and gibbsite (Gb). (F) Staghorn of hollandite involved by gibbsite in the vermiform duricrust of Apuí (VT). (G and H) Contact between acicular cryptomelane (C) and fragments of hollandite in the massive duricrust Novo Natal (M1). (I) Romanechite (Ro) as boxwork constituting the framework of the protopisolitic duricrust (Pp2) of Novo Natal and filled cavities as botryoidal romanechite.

6.3. Cryptomelane of the massive duricrust of Novo Natal

Cryptomelane, which is most common in the massive duricrust of Novo Natal (CM1), forms needles or heterogeneous mass intergrowths with gibbsite and often coexists with hollandite or botryoidal pyrolusite (Fig. 12H). It contains up to 79% MnO_2, between 4 and 4.5% K_2O (Fig. 13A) up to 5% Al_2O_3 and less than 4% other elements (i.e., SiO_2, Fe_2O_3, Mn_2O_3 PbO, CuO, Na_2O, Co and BaO) (Table A8). According to the formula units based on 16 oxygens and Mn^{4+}/Mn^{3+} calculated assuming full site occupancy, the formula of this cryptomelane is $K_{0.69–0.77}Mn^{3+}_{0.33–0.40}Mn^{4+}_{6.76–6.87}O_{16}$ (Table A9).

6.4. Romanechite of the Beneficente, Holanda and Zé Julião deposits

In the Mn-greywackes of the Beneficente, Holanda and Zé Julião deposits, the romanechite in the matrix is zoned, exhibits boxwork habit (Fig. 12I) and is botryoidal when filling voids. In the duricrusts and colluvial fragments, it is massive and sometimes zoned. It is composed of only Mn_2O_3 (65.58–71.16%) and BaO (16.20–18.47%) (Table A10, Fig. 13A); according to the formula units based on 10 oxygens and Mn^{4+}/Mn^{3+} calculated assuming full site occupancy, its formula is $Ba_{0.63–0.72}Mn^{3+}_{0.64–0.72}Mn^{3+}_{4.04–4.11}O_{10}$ (Table A11).

6.5. Goethite and hematite

These minerals display botryoidal and acicular habits in voids or are massive when they are associated with gibbsite pisoliths and quartz grains. In Apuí and Novo Natal, they record 1.61–6.19% MnO and 1.27–13.31% Al_2O_3, which decreases the amount of recorded Fe_2O_3 (58.11–89.4%) (Table A12) and causes the displacement of the main X-ray reflection (110) in the XR diffractogram. Their SiO_2 contents ($\leq$13.5%) are most likely related to the presence of quartz inclusions.

7. Discussion

7.1. Geochemical features

Different environments (i.e., sedimentary, hydrothermal and lateritic) produce a wide and complex variety of structures, textures, minerals and geochemical features that are assigned to

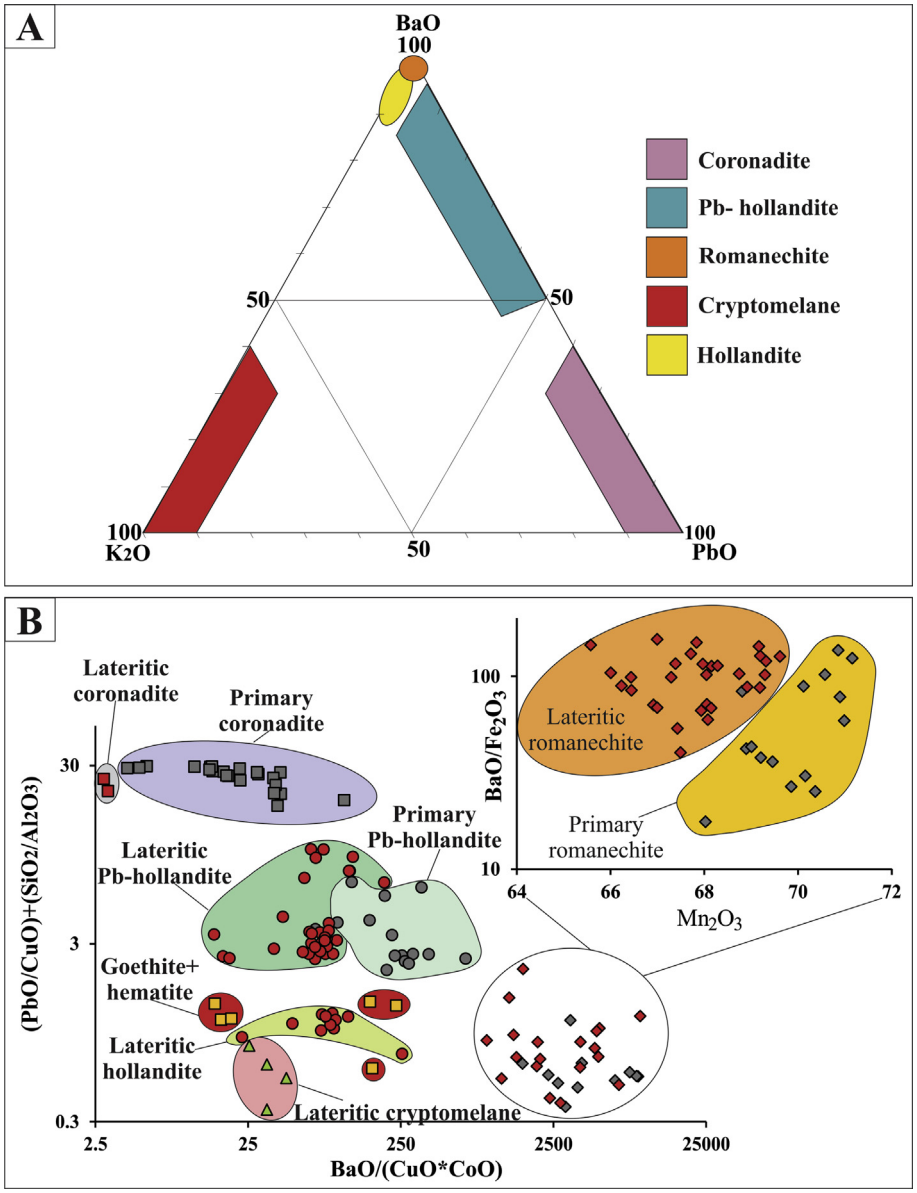

Fig. 13. (A) Ternary diagram K2O-BaO-PbO plot the main Mn-minerals according mineral-geochemistry. (B) A plot that differenciates the primary Mn-minerals from lateritic minerals.

two types of ore: one is related to Novo Natal, Zé Julião and Apui, which record higher concentrations of trace elements and were deposited in a rift basin, and the second one is more pure, is related to Beneficente and Holanda, and was deposited in a post-rift basin. Moving from the sedimentary rock to the lateritic duricrust, the main Mn-minerals of coronadite, hollandite and romanechite changed their chemical compositions and textures. The more mobile elements (MgO, CaO, Na_2O and K_2O) were removed, while the contents of SiO_2, Al_2O_3, Fe_2O_3, MnO, Pb and Co increased. This geochemical change is better shown in Fig. 13B, where the values of BaO/(CuO*CoO) versus (PbO/CuO) + (SiO_2/Al_2O_3) differ between primary coronadite and hollandite and those formed in lateritic conditions. Primary romanechite was distinguished from lateritic romanechite based on their different contents of Mn_2O_3 and BaO/Fe_2O_3 (Fig. 13B). Phosphatic portions (i.e., the solid solution of crandallite-goyazite, sample Pd, Fig 14A) caused P_2O_5 to become trapped in hollandite (Table A6), as well as to form intergrowths with gibbsite, whereas Mn-minerals (Fig. 14B) helped some Al and Mn become trapped in goethite and hematite (1.27–13.31% Al_2O_3 and 1.61–6.19% MnO). The abundance, occurrence and paragenesis of these minerals are shown in Fig. 14C.

The oxidizing environment and the processes of coprecipitation, adsorption, complexation and ion exchange trapped REE within Fe- and Mn-oxides (Braun et al., 1990; Ohta and Kawabe, 2001). In this environment, the reduction of MnO_2 (Mn^{4+} to Mn^{3+} or Mn^{2+}) acted as a catalyst for Ce^{3+} oxidation, forming cerianite and explaining the low contents of Mn^{4+} present in the chemical formulas of hollandite and coronadite (approximately 0.15 and 0.31%, respectively) in studied Mn duricrust relative to Mn-rocks. The reduction of Mn^{4+} to Mn^{3+} also allowed goethite and hematite to trap Mn. Goethite and hematite can also retain Th and Sc; these elements, together with Y, may also be residually concentrated in minerals such as zircon (Middelburg et al., 1988; Kotschoubey et al., 2005; Calagari and Abedini, 2007). These processes explain the association of group 1 (goethite, hematite, gibbsite, Al_2O_3, Fe_2O_3, Sc, Th, Y, U, LOI, Rb, Ce, Pr, Nd, Ho, Er, Tm and Yb) that reg-

ulates most samples of Zé Julião and some samples of the Apuí and Novo Natal duricrusts, which contain more goethite (10–27%), hematite (5–38%) and gibbsite (6–40%) (Fig. 11).

The Ba^{2+} and SO_4^{2-} released in solution from barite, in addition to the availability of MnO_8^{-6} and H_2O, formed romanechite and hollandite as a matrix in the Mn-greywacke (M2), following the equations below:

$$BaSO_4 \rightarrow Ba^{2+}_{(aq)} + SO^{2-}_{4(aq)} \quad (I)$$

$$4H_2O + MnO_8^{-6} \rightarrow Mn^{3+} + 8H^+ + 6O_2 \quad (II)$$

$$2Ba^{2+}_{(aq)} + 5Mn^{3+} + 4H^+ + 6O_2 \rightarrow Ba_2Mn_5O_{10}.2H_2O \quad (III)$$

The repetition of this process created the zoned structures displayed by the romanechite in Mn-greywacke (A2). Although romanechite has a low capacity to scavenge trace elements (Post, 1999; Pracejus and Bolton, 1992), trace elements may become trapped on the surface of romanechite (Ohta and Kawabe, 2001) or within its mineral structure, where Ni^{3+} (0.57 Å), Co^{3+} (0.61 Å) and Mo^{4+} (0.65 Å) can replace Mn^{3+} (0.643 Å) or Mn^{4+} (0.60 Å). These features explain the geochemical association of group 2 (MnO, Ba, Co, Ni, Be, Zn and Mo), which governs the vermiform duricrust of Beneficente and some of the Mn-greywackes and duricrusts of Holanda, Novo Natal and Zé Julião.

Associations 3 and 4 (quartz, coronadite, SiO_2, P_2O_5 and Pb; and Pb-hollandite, cryptomelane, pyrolusite, Ag, As, Cu, Ga, Sr, Tl, Sm, Eu, Gd, Tb and Dy, respectively), mirror most of the Mn-rocks and the lateritic duricrusts of Novo Natal and the Mn layer of Holanda (ML), which is explained by their mineral compositions. Coronadite and hollandite containing PbO and CuO and cryptomelane containing CuO (Tab. A4, A6 and A8) are produced by the remobilization and ability of Pb and Cu to form complexes with Mn, thus creating the several generations of Mn-minerals in the Mn-rocks of Novo Natal (Fig. 12A, B and D). During this process, other elements with geochemical affinities, such as Dy, Tb, Sm, Eu, As, Ag, Cu, Sr and Tl, are also trapped in these minerals, as well as pyrolusite

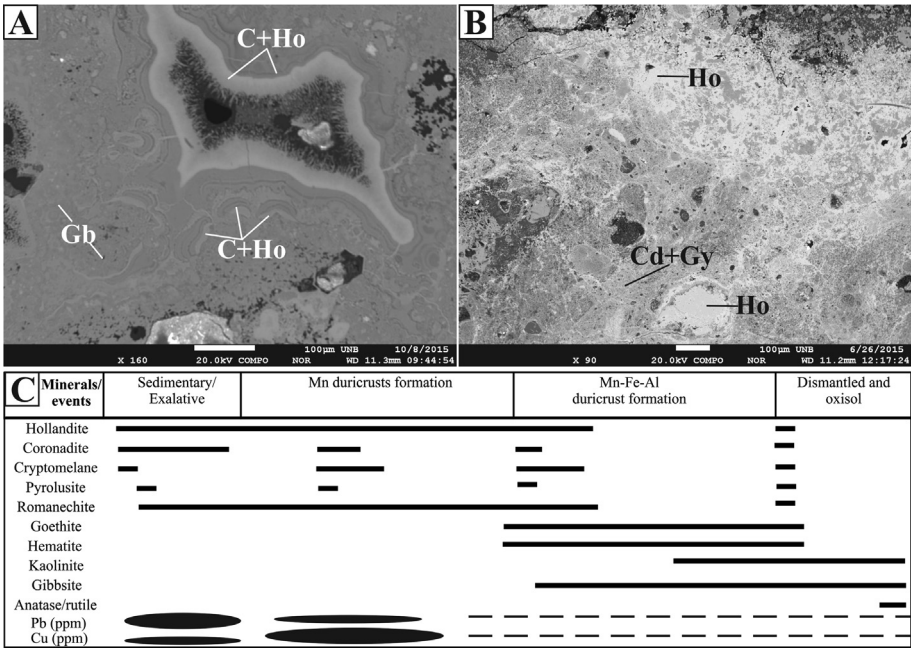

Fig. 14. (A) Detail of the massive duricrust (M1) where gibbsite (Gb- massive dark grey) coexist with relicts of cryptomelane (C) and hollandite (Ho) (light grey and zoned dark grey). (B) Detail of pale grey phosphatic portions (Pd) of the Novo Natal duricrust, where crandallite (Cd) and goyazite (Gy) involving hollandite (light grey). (C) Abundance, mode of occurrence and mineral paragenesis of southwestern Amazonia small Mn deposits.

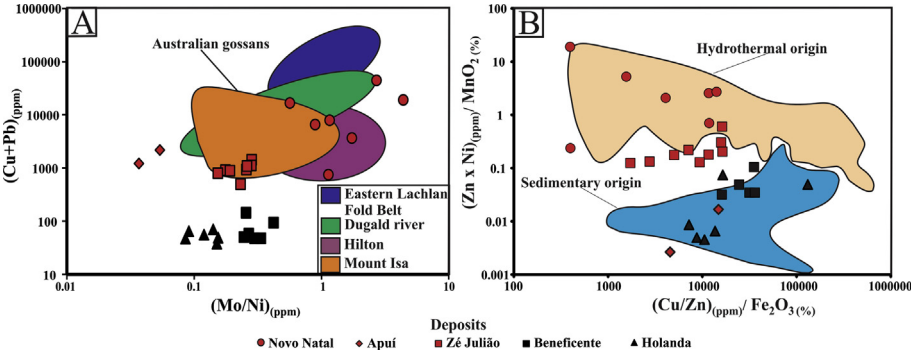

Fig. 15. (A) $(Mo/Ni)_{(ppm)}$ vs $(Cu + Pb)_{ppm}$ comparing the studied deposit with Australian gossans of Taylor and Scott (1982) and Scott et al. (2001). (B) $(Cu/Zn)_{ppm}/Fe_2O_{3(\%)}$ vs $(Zn/Ni)_{ppm}/MnO_{2(\%)}$ comparing the studied deposit with hydrothermal and sedimentary environment of Zantop (1978), Moorby et al. (1984), Bernat et al. (1989), Costa et al. (2005) and Choque Fernandez et al. (2005).

(Pracejus and Bolton, 1992). Gallium in group 4 is related to its immobility or its association with Al-phosphates. Hollandite and coronadite also trap P_2O_5, especially in the Mn-greywacke (A3), where the phosphorous content of both minerals reaches up to 0.37% (Supplementary data files). In the hollandite of the phosphorous portions (sample Pd), the phosphorus content reaches up to 1.05%.

Group 5 (TiO_2, Zr, Hf, La and Nb) mostly identified soils, due to the resistance of rutile and zircon, along with the neoformation of anatase, under the harsher weathering conditions of Amazonia.

7.2. Sedimentary, hydrothermal and geochemical environments

Galena, native silver, coronadite, Pb-hollandite, anomalous Cu and high contents of Tl in the Mn-duricrusts of Novo Natal (45–97 ppm Tl) are similar to those of the gossans described by Calderoni et al. (1985) (which record an average value of 74 ppm). Also, the positive Gd anomalies in Novo Natal and Apuí ($Gd/Gd^* = 1.25–2.15$) are higher, similar to those recorded by the massive sulfides and Mn-deposits with hydrothermal sources ($Gd/Gd^* = 1.3–2.8$, Barrett et al., 1991, Zhao and Jiang, 2007 and Del Rio-Salas et al., 2013). Moreover, the sulfide source of the Novo Natal, Zé Julião and Apuí deposits is also supported by their correlations to the Cu, Pb and Zn concentrations of Australian gossans (Taylor and Scott, 1982; Scott et al., 2001) (Fig. 15A), while evidence of a hydrothermal influence is indicated by their (Zn/Ni)/MnO_2 ratios (Fig. 15B), although Apuí data plot in the sedimentary field. Hence, the Mn of Novo Natal, Zé Julião and Apuí are assigned to the Vila do Carmo Group, which is the Proterozoic volcano-sedimentary sequence of the Apuí region that was deposited in an intracontinental rift basin (Reis et al., 2013) under the influence of sulfide hydrothermal activity. The sulfide hydrothermal activity, which is correlated to the VMS deposits of Cu, Zn, Pb, Ag and Au and gossans (1.78–1.75 Ga) found in this region (i.e., the Juma, Sucunduri and Aripuanã Rivers) (Carvalho and Figueiredo, 1982; Leite et al., 2005 and Brito et al., 2010) are the most likely sources of Mn. This link between Mn and sulfide activity allows us to classify the Mn-deposits of Apuí, Zé Julião and Novo Natal as dubhite (Nicholson, 1992). On the other hand, the Mn-minerals of Beneficente and Holanda, which are more pure, have only a sedimentary source and could thus have been produced by supergene marine/fresh water related to the Beneficente Group, which represents a post-rifting sedimentary sequence (Fig. 15B).

7.3. Provenance of the Mn in the southwestern region of Amazonia

The rocks of the Sunsás, Rondônia Juruena and Tapajós Parima provinces were selected according to the provenance of the sedimentary rocks of the Sumaúma Supergroup postulated by Reis et al. (2013).

The REE/(Zr/Hf) vs $TiO_2 \times 1000/(Co/Ni)$ ratios of the Apuí, Zé Julião and Novo Natal deposits indicate that the felsic volcanic rocks of the Colíder Group and the granitic bodies of the Igarapé das Lontras and Teodósia suites of the Rondônia Juruena and Tapajós Parima provinces were the sources of the Mn of the Vila do Carmo Group (Fig. 16A). The Beneficente and Holanda deposits also record evidence of a felsic source, but are mainly assigned to the Serra da Providência intrusive suite, which records the contribution of the granitic suites of the Sunsás Province (1.45–1.10 Ga) of Santos et al. (2006). The Beneficente deposit also records the mafic rock sources of the Mata-Matá diabase, Serra da Providência, Trincheira Complex and the Nova Brasilândia Group (Fig. 16B). This mafic provenance is also indicated by the observed high contents of Co and Ni and the negative Tb anomalies recorded in the vermiform duricrusts (B2 to B4: $Tb/Tb^* = 0.21–0.33$), which are similar to those recorded in the Mata-Matá diabase ($Tb/Tb^* = 0.21–0.34$; CPRM, 2014).

8. Evolution of manganese and paleoenvironmental implications

The volcanic basement and intrusive granitic bodies (i.e., the Colíder Group and the Teodósia and Igarapé das Lontras intrusive suites), are structured within an intracontinental cratonic Paleoproterozoic rift basin (Reis et al., 2013), which served as a shelter for the rhythmites of the Vila do Carmo Group (Fig. 17A). The Teodósia intrusive suite, which records an average Mn concentration of 1064 ppm (CPRM, 2014) is the most likely source for the Mn of the Mn-greywackes of the Vila do Carmo Group. The downward circulation of warm waters heated by mantle convection (Fig. 17B) brought up Mn, Fe, Ba, Pb, Cu, Ag and Au leached from the VMS orebodies of the volcano-sedimentary rocks. Along fractures and veinlets, coronadite and hollandite formed in the pinkish siltstone (sample PS) of Novo Natal. Meanwhile, the Mn-greywackes (sample A3) overlapped the pinkish siltstone; their primary mineralogy was modified by hydrothermal activity, which formed hollandite in the matrix and coronadite and Pb-hollandite along fractures. This environment is similar to those found in Mn

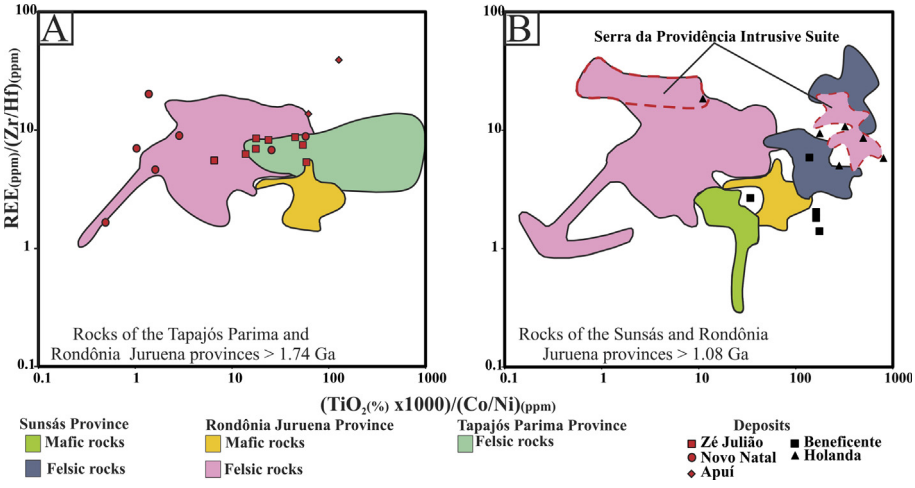

Fig. 16. (A and B) Provenance of the Mn Vila do Carmo and Beneficente Group, respectively, using ($TiO_2 \times 1000$)/(Co/Ni) vs REE/(Zr/Hf) data. The lithostratigraphic units are from Payolla (1994), Rizzotto (1999), Barros (2007), Valério et al. (2009), Brito et al. (2010), Rizzotto and Hartmann (2012), Scandolara et al. (2013), Barreto et al. (2014), CPRM (2014) and Da Silva et al. (2014).

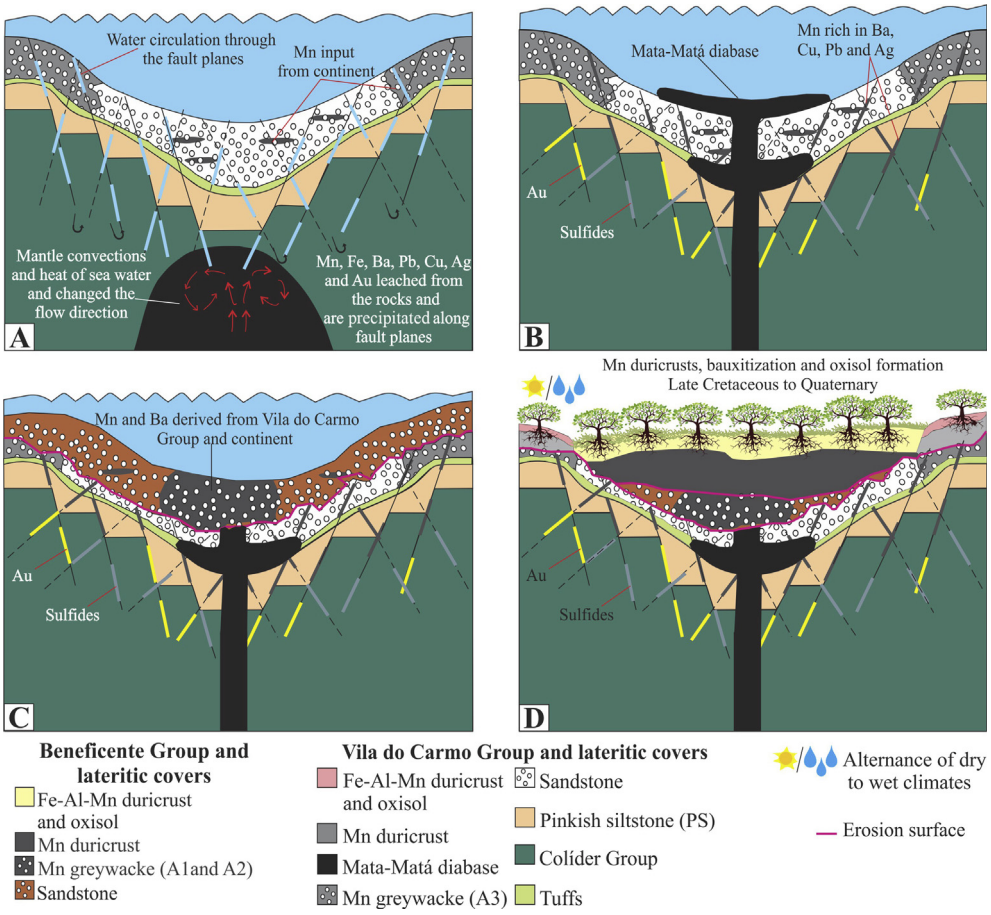

Fig. 17. Schematic evolution of the Mn ore in southwestern of Amazonia. (A) deposition of the volcano-sedimentary rocks of Vila do Carmo Group sediments in a paleoproterozoic rifte basin. Mantelic convection heat the sea water leaching Mn, Fe, Ba, Pb, Cu, Ag and Au from the volcano-sedimentary stacking. (B) Along the fault Mn, Cu and Pb as well as Au and sulfides were precipited. After that, mafic sills and dykes of Mata-Matá diabase (1576 Ga) intersected the volcano-sedimentary stacking. (C) Erosion followed by deposition of Beneficente Group during the Mesoproterozoic where Vila do Carmo Group and Mata-Matá diabase are the main source of Mn for the sediments. (D) Aggressive weathering with formation of lateritic crust during the Cenozoic.

deposits in Mexico (Freiberg, 1983), Greece (Liakopoulos et al., 2001) and India (Ghosh et al., 2015).

After the intrusion of sills and dykes of the Mata-Matá diabase into the Vila do Carmo Group, which was linked to mantle convection, erosional events occurred (as is indicated by the presence of angular discordance) (Reis et al., 2013) (Fig. 17C), and the Beneficente Group was deposited in a coastal Mesoproterozoic environment under the influence of fluvial channels (during the post-rift phase) (Fig. 17C). The erosion of the surrounding rocks, which were mostly granitic suites (i.e., the Sunsás Province and Serra da Providência intrusive suites) and the Vila do Carmo Group, with some contributions of the Mata-Matá diabase and mafic rocks from the Sunsás Province, represented the sources for the Mn of the Beneficente and Holanda deposits.

The presence of Paleozoic and Cenozoic sediments helped to partially protect the Proterozoic sedimentary rocks from erosion. However, when exposed to a drier climate following the Late Cretaceous, lateritic duricrusts with a large diversity of textures (i.e., massive, pisolitic, protopisolitic and vermiform) were formed (Fig. 17D). The most mobile elements were released, and new phases of coronadite, hollandite, cryptomelane and romanechite, which maintained the hydrothermal signature of the Vila do Carmo Group (i.e., the Novo Natal, Apuí and Zé Julião deposits) and the sedimentary signature of the Beneficente Group (i.e., the Holanda and Beneficente deposits), were formed. Concomitant to the transformations of the Mn-minerals and the accumulation of Mn, gibbsite was neoformed in the upper portion of the duricrust, as were goethite, hematite and kaolinite, based on the weathering of clastic minerals, which increased the present amounts of Fe_2O_3 and Al_2O_3 in accordance with the bauxitization process that affected all rocks within the region (Albuquerque and Horbe, 2015). The reactivation of normal faults and the incision of large rivers (i.e., Aripuanã, Sucunduri and Jatuarana) dissected the relief, degraded the duricrust and formed the Mn duricrust colluvium in Zé Julião and the Mn gravels spread throughout the region.

9. Conclusions

The Mn deposits of Novo Natal, Apuí and Zé Julião, which contain unusual amounts of Pb, Cu, Tl and Ag, were produced in the Proterozoic during a rift stage in a sedimentary environment belonging to the Vila do Carmo Group, which was supplied by volcanic and granitic rocks under the influence of hydrothermal activity. Additionally, the post-rift basin, which was supplied only by mafic and felsic rocks, experienced a second Mn deposition event, which produced the Beneficente and Holanda deposits. Lateritization formed duricrusts, and new generations of coronadite, hollandite, cryptomelane and romanechite inherited the geochemical signatures of the Mn-rocks. The preservation of duricrust in Apuí and Zé Julião as plateaus and in Holanda, Beneficente and Novo Natal as lower dissected relief occurred due to the erosion

promoted by the incision of large rivers and neotectonic activity during the Cenozoic.

Although this study was performed to identify the two geological environments of these Mn deposits, the Beneficente Group is the best target for future Mn geological surveys, due to the fact that it covers the largest area and records the most local hydrothermal processes. However, the influences of hydrothermal and sulfide activity identified in Novo Natal, Zé Julião and Apuí, based on the presence of high concentrations of Pb and its Gd and Tl anomalies, indicate that these areas represent good targets for VMS deposits.

Acknowledgments

The authors thank to the Postgraduate Program in Geology from the University of Brasilia, to CAPES for granting a PhD scholarship to the first author and CNPq for financial support (process n ° 471971/2010-3 and 473359/2012) and research grants of the second and third authors. We also thank the anonymous referees that provided helpful suggestions for improving the manuscript.

Appendix A. Supplementary data

Supplementary data associated with this article can be found, in the online version, at http://dx.doi.org/10.1016/j.oregeorev.2017.06.012.

References

Albuquerque, M.F.S., Horbe, A.M.C., 2015. Mineralogia, geoquímica e evolução da lateritização em Apuí, sudeste do Amazonas. Braz. J. Geol. 45, 569–590.

Barreto, C.J.S., Lafon, J.M., Costa, L.T.R., Lima, E.F., 2014. Paleoproterozoic (~1.89 Ga) felsic volcanism of the Iricoumé Group, Guyana Shield, South America: geochemical and Sm-Nd isotopic constraints on sources and tectonic environment. Int. Geol. Rev. 56, 1332–1356.

Barrett, T.J., Cattalani, S., Maclea, W.H., 1991. Massive sulfide deposits of the Noranda area, Quebec. I. The Horne mine. Can. J. Earth Sci. 28, 465–488.

Barros, A.J.P., 2007. Granitos da região de Peixoto de Azevedo – Novo Mundo e mineralizações auríferas relacionadas – Província Aurífera Alta Floresta (MT). PhD thesis, Campinas, Brazil, Universidade Estadual de Campinas, p. 154.

Bernat, M., Causse, C., Perseil, E.A., Feraud, G., 1989. Variations of element distribution in ferromanganese nodules and its bearing on growth rates. Miner. Deposita 24, 258–269.

Betiollo, L.M., Reis N.J., Almeida, M.E., Bahia, R.C., Splendor, F., Costa, U.P., Luzardo, R., 2009. Magmatismo Máfico, Calimiano (Sill Mata-Matá), rio Aripuanã, Amazonas- Implicações Geológicas. In: XI Simpósio de Geologia da Amazônia, Resumos Expandidos.

Braun, J., Pagel, M., Muller, J., Bilong, P., Michard, A., Guillet, B., 1990. Cerium anomalies in lateric profiles. Geochim. Cosmochim. Acta 54, 781–795.

Brito R.S., Silveira F.V., Larizzati J.H., 2010. Metalogenia do distrito aurífero do rio Juma- Nova Aripuanã-AM. Informe recursos minerais. Série Ouro, Brasília, CPRM.

Calagari, A.A., Abedini, A., 2007. Geochemical investigation on Permo-Triassic bauxite horizon at Kanisheeteh, east of Bukan, west-Azarbaidjan, Iran. J. Geochem. Explor. 94, 1–18.

Calderoni, G., Ferrini, V., Masi, U., 1985. Distribution and significance of Pb and Tl in the sulfides and host rocks from hydrothermal mineralization of the Tolfa Mountains (Latium, Central Italy). Chem. Geol. 51, 29–39.

Carvalho, M.S., Figueiredo, A.J., 1982. Caracterização Litoestratigráfica da Bacia de Sedimentação do Grupo Beneficente no Alto Rio Sucundurí-AM. 1st Amazon Geology Symposium, Belém, Brazil, Extended Abstracts, pp. 26–44.

Chisonga, B.C., Gutzmer, J., Beukes, N.J., Huizenga, J.M., 2012. Nature and origin of the protolith succession to the Paleoproterozoic Serra do Navio manganese deposit, Amapa Province, Brazil. Ore Geol. Rev. 47, 59–76.

Choque Fernandez, O.J., Costa, M.L., Pollmann, H., Ribeiro, P.A., Silva, N.C., 2005. Contribuições mineralógicas e geoquímicas sobre a origem do minério de manganês do Morro do Urucum (Corumbá, Brasil): 1st Brazilian Symposium of Metallogeny, Gramado, Brazil, Extended Abstracts, pp. 1–4.

Conly, A.G., Scott, S.D., Bellon, H., 2011. Metalliferous manganese oxide mineralization associated with the Boleo Cu-Co-Zn district, Mexico. Econ. Geol. 106, 1173–1196.

Cornell, D.H., Schutte, S.S., 1995. A volcanic-exhalative origin for the world's largest (Kalahari) manganese field. Miner. Deposita 30, 146–151.

Costa, M.L., Choque Fernandez, O.J., Requelme, M.E.R., 2005. Depósito de manganês do Azul, Carajás: estratigrafia, mineralogia, geoquímica e evolução geológica, In: Marini, O.J., Queiroz, E.T., Ramos, B.V., (Eds.). Caracterização de depósitos minerais em distritos mineiros da Amazônia. Departamento Nacional de Producao Mineral, Fundo Setorial de Recursos Minerais-Agencia para Desenvolvimento Tecnico da Industria Mineral Brasileira (ADIMB), Brasilia, pp. 227–333.

CPRM, 2013. Folha Sumaúma (SB.20-Z-D). Programa Geologia do Brasil. Carta geológica ao milionésimo-Escala 1:250.000. CPRM, Serviço Geológico do Brasil, Manaus.

CPRM, 2014. Geologia e recursos minerais da Folha Sumaúma – SB.20-Z-D, Estado do Amazonas, escala 1:250.000. CPRM, Serviço Geológico do Brasil, Manaus. Programa Geologia do Brasil – PGB. Levantamentos Geológicos Básicos do Brasil.

Da Silva, F.R., Barros, M.A.S., Pierosan, R., Pinho, F.E.C., Rocha, M.L.B., Vasconcelos, B. R., Dezula, S.E.M., Tavares, C., Rocha, J., 2014. Geoquímica e geocronologia U-Pb (SHRIMP) de granitos da região de Peixoto de Azevedo: Província Aurífera Alta Floresta, Mato Grosso. Braz. J. Geol. 44, 433–455.

Del Rio-Salas, R., Ochoa-Landín, L., Eastoe, C.J., Ruiz, J., Meza-Figueroa, D., Valencia-Moreno, M., Zúñiga-Hernández, H., Zúñiga-Hernández, L., Moreno-Rodríguez, V., Mendívil-Quijada, H., 2013. Genesis of manganese oxide mineralization in the Boleo region and Concepción Peninsula, Baja California Sur: constraints from Pb-Sr isotopes and REE geochemistry. Ver. Mex. Cienc. Geol. 30, 482–499.

Force, E.R., Paradis, S., Simandl, G.J., 1999. Sedimentary manganese, in selected British Columbia mineral deposit profiles. In: Simandl, G.J, Hora, Z.D., Lefebure, D.V. (Eds.), Industrial Minerals, London, British Columbia Geological Survey Open-file, pp. 47–50.

Frakes, L., Bolton, B., 1992. Effects of ocean chemistry, sea level, and climate on the formation of primary sedimentary manganese ore deposits. Econ. Geol. 87, 1207–1217.

Freiberg, D.A., 1983. Geologic setting and origin of the Lucifer manganese deposit, Baja California Sur, Mexico. Econ. Geol. 78, 931–943.

Ghosh, R., Chakraborty, D., Halder, M., Baidya, T.K., 2015. Manganese mineralization in Archean greenstone belt, Joda-Noamundi sector, Noamundi basin, East Indian Shield. Ore Geol. Rev. 70, 96–109.

Glasby, G.P., Papavassiliou, C.T., Liakopoulos, A., Galanopoulos, V., 2001. Past mining of the Vani manganese deposit, Milos Island, Greece. 5th International Mining History Congress, Milos, pp. 93–105.

Gonçalves, E., Serfaty, A., 1976. Perfil analítico do manganês. Departamento Nacional da Produção Mineral/DNPM, Brasília.

Gutzmer, J., Beukes, N.J., 1996. Mineral paragenesis of the Kalahari manganese field, South Africa. Ore Geol. Rev. 11, 405–428.

Kotschoubey, B., Truckenbrodt, W., Calaf, J.M.C., 2005. Evolução Geológica da Porção Meridional da Província Bauxitífera de Paragominas durante o Neógeno/Pleistoceno (Noroeste da Bacia do Grajaú, Nordeste do Pará e Extremo oeste do Maranhão). Braz. J. Geol. 35, 263–272.

Leal, P.R., Correa, M.J., Ametrano, S.J., Etcheverry, R.O., De Brodtkorb, M.K., 2008. The manganese deposits of the Pampean Ranges, Argentina. Can. Mineral 46, 1215–1233.

Leite, J.A.D., Sousa, M.Z.A., Saes, G.S., Macambira, M.J.B., Xavier, R.P., Siqueira, A.J., Batata, M.E.F., Oliveira, F.A., Silva Jr, J.G., Quadros, A.P., 2005. Caracterização do Depósito Polimetálico (Zn, Pb, Ag, Cu-Au) de Aripuanã, Mato Grosso. In: Marini, O. J., Queiroz, E. T., and Ramos, B.V. (Eds.), Caracterização de depósitos minerais em distritos mineiros da Amazônia, Brasilia, Departamento Nacional de Producao Mineral, Fundo Setorial de Recursos Minerais-Agencia para Desenvolvimento Técnico da Industria Mineral Brasileira (ADIMB), pp. 601–686.

Liakopoulos, A., Glasby, G.P., Boulegue, J., 2001. Nature and origin of the Vani manganese deposit, Milos, Greece: an overview. Ore Geol. Ver. 18, 181–209.

Liberatore, G., Alecrim, J.D., Medeiros, J.B., Malouf, R.F., Pinheiro, S.S., Achão, S.M., Santos, J.O.S., 1972. Projeto Aripuanã – Sucundurí, DNPM/CPRM, Manaus.

Maynard, J.B., 2014. Manganiferous Sediments, Rocks, and Ores. In: Holland, H.D., Turekian, K.K. (Eds.), Treatise on Geochemistry, Second Edition. Elsevier, pp. 327–349.

Maynard, J.B., 2010. The chemistry of manganese ores through time: a signal ofincreasing diversity of earth – surface environment. Econ. Geol. 105, 535–552.

Middelburg, J.J., Van Der Weijden, C.H., Woittiez, J.R.M., 1988. Chemical processes affecting the mobility of major, minor and trace elements during weathering of granitic rocks. Chem. Geol. 68, 253–273.

Moorby, S.A., Cronan, D.S., Galsby, G.P., 1984. Geochemistry of hydrothermal Mn-oxide deposits from the S.W. Pacific island arc. Geochim. Cosmochim. Acta 48, 433–441.

Nicholson, K., 1992. Contrasting mineralogical-geochemical signatures of manganese oxides: guides to metallogenesis. Econ. Geol. 87, 1253–1264.

Nicholson, K., Nayak, V.K., Nanda, J.K., 1997. Manganese ores of the Ghoriajhor Monmunda area, Sundergarh District, Orissa, India: geochemical evidence for a mixed Mn source. In: Nicholson, K., Hein, J.R., Buhn, B., Dasgupta, S. (Eds.), Manganese Mineralization: Geochemistry and Mineralogy of Terrestrial and Marine Deposits. Geological Society, London, pp. 117–121. Special Publication.

Ohta, A., Kawabe, I., 2001. REE (III) adsorption onto Mn dioxide (d-MnO_2) and Fe oxyhydroxide: Ce (III) oxidation by d-MnO_2. Geochim. Cosmochim. Acta 65, 695–703.

Okita, P.M., 1992. Manganese carbonate mineralization in the Molango District, Mexico. Econ. Geol. 87, 1345–1366.

O'Reilly, G.A., 1992. Petrographic and Geochemical Evidence for a Hypogene Origen of Granite- Hosted, Vein Type Mn Mineralization at the New Ross Mn Deposits, Lunenburg County, Nova Scotia. Can. Econ. Geol. 87, 1275–1300.

Payolla, B.L., 1994. As rochas graníticas e sieníticas das cachoeiras Teotônio e Santo Antônio, rio Madeira, Porto Velho, Rondônia: geologia, petrografia e geoquímica. Msc thesis, Brasília, Brazil, Universidade de Brasília, p. 145.

Post, J.E., 1999. Manganese oxide minerals crystals structures and economic and environmental significance. Proc. Natl. Acad. Sci. U.S.A. 96, 3447–3454.

Pracejus, B., 1989. Nature and formation supergene manganese deposits on Groote Eylandt, N.T., Australia, Unpublished. Ph.D thesis, Adelaide University, p. 231.
Pracejus, B., Bolton, B.R., 1992. Geochemistry of supergene manganese oxide deposits, Groote Eylandt. Aust. Econ. Geol. 87, 1310–1335.
Reis, N.J., Bahia, R.B.C., Almeida, M.E., Costa, U.A.P., Betiollo, L.M., de Oliveira, A.C., Splendor, F., 2013. O supergrupo Sumaúma no contexto geológico da Folha SB.20-Z-D (SUMAÚMA), sudeste do Amazonas: modo de ocorrência, discussão de idades em zircões detríticos e correlações no SW do Cráton do Amazonas. In: Wankler, F.L., Holanda, E.C., Vasques, M.L. (Eds.), Contribuições à Geologia da Amazônia, Belém, pp. 199–222.
Rizzotto, G.J., 1999. Petrologia e geotectônica do Grupo Nova Brasilândia, Rondônia. Msc thesis. Porto Alegre, Brazil, Federal University of Rio Grande do Sul, p. 131.
Rizzotto, G.J., Hartmann, L.A., 2012. Geological and geochemical evolution of the Trincheira Complex, a mesoproterozoic ophiolite in the southwestern Amazon Craton, Brazil. Lithos. 148, 277–295.
Rodrigues, O.B., Kosuki, R., Coelho Filho, A., 1986. Distrito manganesífero de Serra do Navio, Amapá. In: Schobbenhaus, C., Coelho, C.E.S. (Eds). Principais Depósitos Minerais do Brasil, DNPM/CVRD, pp. 167–175.
Roy, S., 1992. Enviroments and process of manganese deposition. Econ. Geol. 87, 1218–1236.
Roy, S., 1997. Genetic diversity of manganese deposition in the terrestrial geological record, In: Nicholson, K., Hein, J., Bühn, B., Dasgupta, S. (Eds.). Manganese Mineralisation: Geochemistry and Mineralogy of Terrestrial and Marine Deposits, Special Publication—Geological Society of London, London, pp. 5–27.
Roy, S., 2006. Sedimentary manganese metallogenesis in response to the evolution of the Earth system. Earth-Sci. Rev. 77, 273–305.
Roy, S., Purkait, P.K., 1968. Mineralogy and genesis of the metamorphosed manganese silicate rocks (gondite) of Gowari Wadhona, Madhya Pradesh, India. Contrib. Mineral. Petr. 20, 86–114.
Santos, J.O.S., 2003. Geotectônica dos Escudos das Guianas e Brasil Central. In: Bizzi, L.A., Schobbenhaus, C., Vidotti, R.M., Gonçalves, J.H. (Eds.). Geologia, Tectônica e Recursos Minerais Minerais do Brasil: texto, mapas e SIG. CPRM- Serviço Geológico do Brasil, pp. 169–226.
Santos, J.O.S., Hartmann, L.A., Faria, M.S.G. de, Riker, S.R.L., Souza, M.M. de, Almeida, M.E., McNaughton, N.J., 2006. A compartimentação do Cráton Amazonas em Províncias: Avanços ocorridos no período 2000–2006. In: SBG- Núcleo Norte, Simp. Geol. Amaz., 9, Belém, PA, Resumos Expandidos.CD-Rom.
Scandolara, J.E., Fuck, R.A., Dall'Agnol, R., Dantas, E.L., 2013. Geochemistry and origin of the early Mesoproterozoic mangerite-charnockite-rapakivi granite association of the Serra da Providência suite and associated gabbros, central-eastern Rondônia, SW Amazonian Craton, Brasil. J. South Am. Earth Sci. 45, 166–193.
Scott, K.M., Ashley, P.M., Lawie, D.C., 2001. The geochemistry, mineralogy and maturity of gossans derived from volcanogenic Zn-Pb-Cu deposits in the eastern Lachlan Fold Belt, NSW. Aust. J. Geochem. Explor. 72, 169–191.
Silva, P.J.M., Horbe, A.M.C., Horbe, M.A., 2012. Mineralogia e geoquímica de ocorrências manganesíferas da bacia Alto Tapajós, sudeste do Amazonas, Brasil. Bol. Mus. Para. Emílio Goeldi. Cienc. Nat. 7, 11–28.
Taylor, G.F., Scott, K.M., 1982. Evaluation of mineralisation Queensland gossans in relation to lead-zinc in the Mount Isa Inlier, Queensland. J. Aust. Geol. Geophys. 7, 159–180.
Taylor, S.R., McLennan, S.M., 1985. The continental crust: its composition and evolution. An Examination of the Geochemical Record Preserved in Rocks. Blackwell Scientific Publications, Oxford.
Valério, C.S., Souza, V.S., Macambira, M.J.B., 2009. The 1.90–1.88 Ga magmatism in the southernmost Guyana Shield, Amazonas, Brazil: geology, geochemistry, zircon geochronology, and tectonic implications. J. South Am. Earth Sci. 28, 304–320.
Zantop, H., 1978. Geologic setting and genesis of iron oxides and manganese oxides in the San Francisco manganese deposit, Jalisco, Mexico. Econ. Geol. 73, 1137–1149.
Zhao, K., Jiang, S., 2007. Rare earth element and yttrium analyses of sulfides from the Dachang Sn-polymetallic ore field, Guangxi Province, China: implication for ore genesis. Geochem. J. 41, 121–134.